Photon Factory Activity Report 2001 #19B
–Users' Report–

▶*Atomic and Molecular Science*
▶*Applied Science*
▼***Biological Science***

40 X-ray crystallographic study of V_1-ATPase
Noriyuki ISHII
6A/2001G339

41 Crystal structure analysis of an autoregulator-receptor protein in *Streptomyces* species
Ryo NATSUME, hin MURAOKA, Yutaka FURUSAWA, Toshiya SENDA
6A/2001G346

42 Characterization of transient intermediates of a calmodulin-peptide complex 2
Yoshinobu IZUMI, Yuji JINBO, Tomohiro MATSUFUJI, Hidenori YOSHINO, Yuzuru HIRAGI, Hiroshi KIHARA
10C/2001G366

43 A small angle X-ray scattering study of ClpA and ClpP from *Escherichia coli*
Yoshihiko IGARASHI, Kazumoto KIMURA, Shigeru MATSUZAKI, Hiroshi KIHARA , Singh SATYENDRA, Michael MAURIZI
15A1/2001G368

44 An X-ray solution scattering study on the conformation of skeletal muscle myosin subfragment-1 in the presence of Mn^{2+} and ATP
Tomohiro OKUMURA, Toshiaki ARATA, Yasunobu SUGIMOTO, Yasunori TAKEZAWA, Maya KIYOTOSHI, Katsuzo WAKABAYASHI
15A/2001G369

45 Alteration of the helical twist associated with the shortening of the thin actin filaments upon activation of skeletal muscles
Yasunori TAKEZAWA, Yasunobu SUGIMOTO, Takakazu KOBAYASHI, Kanji OSHIMA, Katsuzo WAKABAYASHI
15A/2001G370

46 Study of uracil DNA glycosylase complexes with ligands by synchrotron X-ray scattering
Alexander TIMCHENKO, Elena KUBAREVA, Hiroshi KIHARA
15A1/2001G372

47 Fibrillation of human calcitonin as studied by solution x-ray scattering
Tadashi TOMIZAWA, Yasutaka SEKI, Yuzuru HIRAGI, Kunitsugu SODA
10C/2001G375

48 Analysis of unfolding and refolding of HIV protease
Kayoko TAKEUCHI, Hiroyuki KOGO, Hideshi INOUE, Yon-Tae KIM, Xin-Li LIN, Yoshiyuki AMEMIYA, Hiroshi KIHARA, Masaki KOJIMA, Kenji TAKAHASHI
15A/2001G376

49 Improvement of spatial resolution in soft X-ray microscope
Atsushi ITO, Kunio SHINOHARA, Toshio HONDA, Misako SAITO, Rumiko KURIYAMA, Hideyuki YOSHIMURA, Hiroshi MAEDA, Ayumi HORI, Hisamitsu ENDOH, Takashi KOMATSUBARA, Masato ACHIHARA, Yasuhito KINJO
11A/2001G378

50 Changes in the diffraction patterns of hair samples resulting from increased airport and postal security checks post September 11, 2001.
Veronica JAMES
15A/ANBF

6A, 6B/1999G302

X-ray crystallographic studies of group II chaperonin from hyperthermophilic archaea

Yasuhito SHOMURA,[1] Takao YOSHIDA,[2] Tadashi MARUYAMA,[2]
Masafumi YOHDA,[3] and Kunio MIKI*[1,4]
[1]Department of Chemistry, Graduate School of Science, Kyoto University,
Sakyo-ku, Kyoto 606-8502, Japan
[2]Marine Biotechnology Institute, Co. Ltd.,
Kamaishi Laboratories, 3-75-1 Heita, Kamaishi, Iwate 026-0001, Japan
[3]Department of Biotechnology and Life Sciences, Tokyo University of Agriculture & Technology,
2-24-16 Naka-cho, Koganei, Tokyo 184-8588, Japan
[4]RIKEN Harima Institute/SPring-8,
Koto 1-1-1, Mikazukicho, Sayo-gun, Hyogo 679-5148, Japan

Introduction

Chaperonins, ubiquitous folding chambers for newly synthesized or denatured proteins, have been divided into two groups. GroEL from *Escherichia coli*, whose properties have been well studied, is a member of group I chaperonins, and the chaperonins from other species of eubacteria and endosymbiotic organelles also belong to the group I. On the other hand, group II chaperonins exist in archaebacteria, and the eukaryotic cytosl. As a one of major differences between two groups, group I chaperonins requires a single ring cofactor (termed as GroES in *Escherichia. coli*) for enclosing its cavities, while group II chaperonins have built-in lid segment by itself, and no homologue of the cofactor has been found. Moreover, most of the group I chaperonins consist of double homo-heptameric ring whereas group II chaperonins are found in archaea and cytoplasm of eukaryotes. Up to now, there is less knowledge about the mechanism of group II chaperonin.

The G65C/I125T mutant of α subunit hexadecamers of the group II chaperonin from *Thermococcus* strain KS-1 shows activities for ATP hydrolysis and capturing denatured proteins, but is unable to refold them in ATP depending manner, although the wild type of the recombinant α hexadecamer of this chaperonin has all three activities.

Materials and Method

α subunit hexadecamer from *Thermococcus* KS-1 was overexpressed in *E.coli*, purified and crystallized as described [1]. Diffraction data was collected at 100 K at the Photon Factory (BL6A and BL6B). Initial phases were obtained with the molecular replacement using the previously determined crystal structure of α subunit of archaeal chaperonin from *Thermoplasma acidophilum* as a model. After the crystallographic refinement using the program CNS, R_{work} and R_{free} were reduced 26.8 % and 28.9 %, respectively.

Results and Discussion

The crystal structure of mutant (G65C/I125T) α chaperonin from *Thermococcus* KS-1 was determined at 2.8 Å resolution by the molecular replacement method. The overall structure is composed of two stacked rings, each of which is comprised of eight α subunits, with the height of 156 Å and the diameter of 159 Å. Four α subunits are included in an asymmetric unit with the space group $P42_12$. Of these four α subunits, two consist in one ring, and the others two are in the opposite ring. The 8-fold axis in the hexadecamer of the chaperonin is consistent with a crystallographic 4-fold axis.

The whole structure has a spherical aspect and entrances of the cavities are completely closed with hydrophilic environment providing into the cavity, which is considered as a refolding active form for denatured proteins. This result seemed to be strange, since this mutant had already been shown to defects refolding activities *in vitro*. But, comparison of the present structure with the GroEL structure revealed that substituted residue (G65C) should affect on the conformational rearrangement for a refolding cycle. Namely, the side chain of cystein at the 65th position is too balky to allow the chaperonin to undergo local conformational changes, which lead drastic conformational change later in the course of the ATP-depending cycle.

References

[1] Y. Shomura, T. Yoshida, T. Maruyama, M. Yohda, and K. Miki, Acta Crystallogr., Sect. D, submitted.

* miki@kuchem.kyoto-u.ac.jp

15A/1999G328

X-ray diffraction studies on light induced structural changes of cephalopod visual cells

Toshiaki HAMANAKA*[1], Masatsugu SEIDOU[2], Kinya NARITA[3], Masanao MICHINOMAE[4], Yasunobu SUGIMOTO[1], Katsuzo WAKABAYASHI[1] and Yoshiyuki AMEMIYA[5]
[1]Department of Systems and Human Science, Graduate School of Engineering Science, Osaka University, Toyonaka, Osaka 560-8531, Japan.
[2]Department of General Education, Aichi Prefectural University of Fine Arts and Music, Nagakute, Aichi 480-1194, Japan.
[3]Department of Biology, Faculty of Science, Toyama University, Toyama, Toyama 930-8555, Japan.
[4]Department of Biology, Faculty of Science, Konan University, Kobe, Hyogo 658-0072, Japan.
[5]Graduate School of Frontier Sciences, The University of Tokyo, Hongo, Bunkyo, Tokyo 113-8656, Japan.

Introduction

The initial step of the visual process is the absorption of light by the visual pigment. The cephalopod visual pigment is located in microvilli which are cylindrical extensions of the cell membrane, arranged hexagonally within the rhabdome. Previously, the squid retinas fixed by glutaraldehyde was used, because this tissue disintegrated within 1 hour of dissection. It has been reported that we could succeed in recording the x-ray diffraction pattern from unfixed retina by use of the synchrotron radiation and a storage phosphor screen, the imaging plate[1]. Also, we have reported the some change of diffraction pattern induced in response to the light stimulation[2].

In the previous study[3], we showed that the lattice dimension of hexagonally arranged microvilli decreased upon the light illumination and recovered to the original one in the dark about ten minutes after the light stimulation. In this study, we have tried to follow the change of diffraction pattern after the light illumination by use of a CCD-based x-ray detector

Experimental

Living, active specimens of the squid, Watasenia scintillans were captured at Toyama Bay of the Japan sea and brought to Tsukuba within several hours. The squids were decapitated and their retinas dissected in dim red light. For the x-ray experiment, a 1-mm thick slice of retina was kept in an artificial seawater chamber with Mylar windows at 4 C. Schematic diagram of a slice of squid retina was shown in the previous report[1]. The artificial sea water containing D-glucose was oxygenated and gently circulated through the sample chamber during the experiment. Blue light emitted LED was used for light stimulation (465 nm in wavelength).

X-ray experiments have been performed with a mirror –monochromator optics (the Muscle Diffractometer) at BL-15A1[4]. The wavelength of radiation was 0.150 nm. The sample-to-detector distance was 2092 mm. X-ray diffraction intensity was recorded with a CCD-based x-ray detector system[5]. X-ray diffraction data were successively taken on the same sample in the dark and /or light. The exposure time was 1 seconds usually and 40 ms for time resolved experiments and each recording finished within 30 minutes after decapitation.

Results and Discussion

The present study confirmed the change of lattice dimension upon the light illumination observed in the previous studies. However, the lattice dimension became irreversibly larger than the original one after the recovery and the quality of the diffraction pattern deteriorated concomitantly. Sometimes the increase of the lattice dimension started at the early stage after the light stimulation. The similar increase was also observed in the unilluminated retina. These results suggest that the decrease of the lattice dimension in response to the light stimulation may be related to the visual excitation. But the increase of the lattice dimension may correspond to the disintegration of the tissue by the radiation damage and/or the autolysis. Time resolved experiment with 40 ms time slices could not indicate significant changes of diffraction pattern due to partly the low signal to noise ratio.

References

[1] T. Hamanaka et al., PF Activity Report, No.6 124 (1988).
[2] T. Hamanaka et al., PF Activity Report, No.7 131 (1989)
[3] T. Hamanaka et al., PF Activity Report, No.17(Pt.B) 241 (1999)
[4] Y. Amemiya et al., Nucl. Instrum. Methods, 208, 471 (1983)
[5] Y. Amemiya et al., Rev. Instrum. Methods, 66, 2290 (1995)

* hamanaka@bpe.es.osaka-u.ac.jp

15A, 1999G333

Small-angle X-ray scattering study of amyloid fibril formation of hen egg white lysozyme

Yasushige Yonezawa[1], Shinpei Tanaka[2], Tomomi Kubota[3], Katsuzo Wakabayashi[4], Katsuhide Yutani[5], and Satoru Fujiwara[6]*

[1]Tsukuba College Tech., Tsukuba, Ibaraki 305-0821, Japan,
[2]Special Div. Human Life Tech., AIST, Ikeda, Osaka 563-8577,
[3]Inst. Mol. Cell Biol., AIST, Central 2, 1-1-1 Umezono, Tsukuba, Ibaraki 305-8568, Japan,
[4]Div. Biophys. Eng., Osaka Univ., Toyonaka, Osaka 560-8531, Japan,
[5]Inst. Protein Res., Osaka Univ., Yamadaoka, Osaka 565-0871, Japan,
[6]ASRC, JAERI, Tokai-mura, Naka-gun, Ibaraki 319-1195, Japan

Introduction

Hen egg white lysozyme (HEWL) has been known to form amyloid fibrils [1,2]. Since HEWL is one of the proteins that have been studied most extensively and closely related to human lysozyme, the variants of which form the amyloid fibrils [3,4], this protein is an ideal model to study the mechanism of the amyloid fibril formation. HEWL was shown to form the amyloid fibrils in highly concentrated ethanol solutions [1]. In order to gain an insight into the mechanism of the amyloid fibril formation, structural states of HEWL under solutions of various HEWL concentrations in various ethanol concentrations were investigated with small-angle X-ray scattering.

Materials and Methods

Hen egg white lysozyme, purchased from Seikagaku Kogyo, was purified as described [1]. Concentrated solution of this purified HEWL was mixed with H_2O and ethanol to obtain the solutions of the desired protein and ethanol concentration. These sample solutions were used in X-ray scattering experiments. Small-angle X-ray scattering experiments were performed at the BL-15A, using monochromatic X-ray beam of the wavelength 0.15 nm, with the sample-to-detector length of 2.33 m. The obtained scattering curves were analyzed to yield the structural parameters, based on the Guinier approximation [5]. The radius of gyration and I(0)/c which is proportional to molecular weight of the particle, and, if the particles were filamentous, the cross-sectional radius of gyration and $I_x(0)/c$ which is proportional to the mass per unit length of the particle, were estimated from the analysis.

Results

We measured small-angle X-ray scattering patterns of HEWL solutions in the concentration ranges between 2 and 10 mg/ml, under various conditions where the ethanol concentration in the solution was between 0% and 90% (v/v). Each scattering pattern was analyzed to yield the structural parameters as mentioned in *Materials and Methods*. From the results of this analysis, the structural states of HEWL were distinguished as the monomer state, the state of the formation of the dimers, the states of the protofilament formation, the protofilament state, and the states towards the formation of the amyloid fibrils. These structural states changed as a function of both the protein concentration and ethanol concentration. It was found that HEWL under the monomer state had an overall shape similar to that without ethanol, and the dimers, formed by the association at the end of the long axis of HEWL, had an elongated shape. The structure of the protofilament was characterized by its radius of gyration of the cross-section of 2.4 nm. Comparison of the mass per unit length of the protofilament with that of f-actin, one of standard filamentous protein complexes, yielded the mass per unit length of the protofilament 16000 ± 2300 daltons/nm. It was shown that these protofilaments were formed in a manner consistent with nucleation dependent polymerization mechanism [6]. It was also shown that the changes of the structural states towards the amyloid fibril formation occured via lateral association of the protofilaments. Thus, the amyloid fibril formation of HEWL occurs with two steps, the formation of the protofilament by a nucleation dependent polymerization mechanism, followed by the formation of the amyloid fibril via lateral association of the protofilaments.

Supported in part by the REIMEI research resources of JAERI.

References

[1] S. Goda et al., Protein Sci. 9, 369 (2000).
[2] M.R.H. Krebs et al., J. Mol. Biol. 300, 541(2000).
[3] M. Pepys et al., Nature, 362, 553 (1993).
[4] J. Funahashi et al., J. Biochem., 120**,** 1216 (1996).
[5] A. Guinier and G. Fournet, *Small-angle scattering of X-rays*, John Wiley & Sons, New York, (1955).
[6] T.R. Serio et al., Science, 289**,** 1317 (2000).

* fujiwara@kotai3.tokai.jaeri.go.jp

6A, 18B/2000G126

Crystal structure of aspartase from *Bacillus* sp. YM55-1

Tomomi FUJII[1], Hisanobu SAKAI[1], Yasushi KAWATA[2], Yasuo HATA*[1]
[1]Inst. for Chem. Res., Kyoto Univ., Gokasho, Uji, Kyoto 611-0011, Japan
[2]Dep. of Biotech., Fac. of Eng., Tottori Univ., Tottori 680-0945, Japan

Introduction

Aspartase (EC 4.3.1.1) plays an important role in bacterial nitrogen metabolism by catalyzing the reversible conversion of L-aspartate to fumarate and ammonium ion. Although the crystal structure of the enzyme from *Escherichia coli*, which is allosterically activated in the presence of Mg^{2+} ion at alkaline pH, has been elucidated, there are little known about the catalytic residues and detailed reaction-mechanism of the enzyme [1].

Recently, a novel thermostable aspartase from *Bacillus* sp. YM55-1 was isolated and characterized using biochemical and biophysical methods [2]. The *Bacillus* sp. YM55-1 aspartase forms a homotetramer and the subunit consists of 468 amino acid residues (M_r = 51,627). The enzyme has a high specific activity without any allosteric behavior and displays much higher resistance to thermal and chemical denaturation than other mesophilic aspartases. In order to obtain structural information on the reaction mechanism of aspartase and the thermostability of the present enzyme, we have determined the crystal structure of the *Bacillus* sp. YM55-1 aspartase at 2.5 Å resolution by X-ray crystallography.

Experimental

The crystals of the enzyme were obtained by a sitting drop vapor diffusion method using PEG4000 and 2-propanol as precipitants at 30°C. Two sets of diffraction data for two crystals (NAT1 and NAT2) were collected on a screenless Weissenberg camera with a imaging plate (400 mm × 200 mm size) at the BL18B station of the Photon Factory. The data collection of NAT1 and NAT2 were performed at 291K with one crystal sealed in a glass capillary and at 100K with a flash-cooled crystal in the liquid nitrogen gas stream, respectively. Both the data sets were processed, scaled and merged with the programs DENZO and SCALEPACK. The crystals belonged to space group $P2_12_12$ with unit cell dimensions of a = 76.21 Å, b = 140.5 Å and c = 101.9 Å for NAT1 with R_{merge} 11.8%, and a = 74.90 Å, b = 139.5 Å and c = 100.2 Å for NAT2 with R_{merge} 10.2%, respectively.

The structure of the present aspartase was determined by a molecular replacement method using coordinates of the *E. coli* aspartase as a starting model, with a technique of searching *R*-factor along the crystallographic *c*-axis using the program X-PLOR. The NAT1 data was used at the first stage of the analysis. One of three pattern-combinations of two subunits selected from four subunits in the molecule shows an apparently high peak for the solution of the rotation function. The model of the subunit dimer rotated based on the solution was translated at intervals of 1.0 Å along the crystallographic *c*-axis over overlaying the molecular two-fold axis on the crystallographic axis. After each translation, the model was refined as a rigid body and the *R*-factor and R_{free}-factor values were calculated in 10–4 Å resolution range. The subunit dimer was transferred to the location giving the minimum values. Calculations of the positional refinement, the solvent flattening, and the density averaging by NCS, and the model building of polypeptide were repeated at 3.0 Å resolution. After the model of the structure was constructed up to about 80%, the NAT2 data set was used instead of the NAT1 data set, and the program CNS with a maximum likelihood target function was used for the refinement. Finally, the refinement of the current model was converged to an *R*-factor of 22.2% and R_{free}-factor of 26.9% at 2.5 Å. The final model of two independent subunits consists of 468 amino acid residues for A- and D-chains and 225 water molecules.

Results and discussion

The *Bacillus* YM55-1 aspartase consists of four subunits arranged by the 222 point symmetry, and each subunit is composed of three domains. The N-terminal large domain (residues 1-139) consists of five helices. The central helix domain (residues 140-393) is composed mainly of six long α-helices. The C-terminal small domain (residues 394-468) is composed of several short helices. The secondary-structure location and the folding pattern in the subunit of the *Bacillus* YM55-1 aspartase are quite similar to those of the *E. coli* aspartase and the *E. coli* fumarase C. However, the overall structure of the subunit of the present enzyme resembles that of the citrate-complexed fumarase C from *E. coli* rather than that of the ligand-free aspartase from *E. coli*.

The main reasons for the thermostability of the *Bacillus* YM55-1 aspartase are the increase of especially intersubunit hydrogen-bonds and ion-pairs, the slight increase of interface area between subunits, and the shortening of turns.

References

[1] W. Shi et al., Biochemistry **36**, 9136 (1997).
[2] Y. Kawata et al., Arch. Biochem. Biophys. **366**, 40 (1999).

* hata@scl.kyoto-u.ac.jp

6A, 18B/2000G130

X-ray crystallographic studies of V-type H^+-ATPase

Nobutaka NUMOTO[1], Terukazu NOGI[1] and Kunio MIKI*[1, 2]

[1]Department of Chemistry, Graduate School of Science, Kyoto University, Sakyo-ku, Kyoto 606-8502, Japan

[2]RIKEN Harima Institute / SPring-8, Koto 1-1-1, Mikazukicho, Sayo-gun, Hyogo 679-5148, Japan

Introduction

V-type H^+-ATPases (V_oV_1-ATPase) and F-type H^+-ATPases (F_oF_1-ATPase) are two subclasses of the ATPase/ATP synthase superfamily. In eukaryotic cells, F_oF_1-ATPases are responsible for ATP synthesis and present in the inner membranes of mitochondria and thylakoid membranes of chloroplasts. In prokaryotic cells, V_oV_1-ATPases are found in the plasma membranes of some archaea and eubacteria. Their physiological role is ATP synthesis coupled with proton flux across the plasma membranes.

Thermus thermophilus is an aerobic thermophilic eubacterium, which has an optimum growth temperature of 343K. It was shown that the plasma membrane H^+-translocating ATPase of *T. thermophilus* belongs to V_oV_1-ATPase. V_oV_1-ATPase from *T. thermophilus* consists of two functional sets of subunits, a peripheral V_1 moiety (V_1-ATPase) and a membrane integrated V_o moiety. The V_1-ATPase has an ATP synthesis/hydrolysis activity and is composed of four subunits, A, B, γ and δ, with a stoichiometry of $A_3B_3\gamma_1\delta_1$. The molecular weight of the V_1-ATPase is estimated to be 400,000. The catalytic sites are located on the A subunits, which are homologous to the β subunits of F_1-ATPases, and has nucleotide binding Walker motifs.

The three-dimensional structures of F_1-ATPases have already been determined at atomic resolution. However, no three-dimensional structures of V_oV_1-ATPases are available. Therefore, the structure determination at high resolution is indispensable for understanding of V_oV_1-ATPases; furthermore, the structural comparison between F_oF_1-ATPases and V_oV_1-ATPases is expected to elucidate the common structural features as biological energy conversion machinery, which couples ATP synthesis/hydrolysis reaction with proton translocation across a membrane.

Results and Discussion

V_1-ATPase from *T. thermophilus* was purified as described [1]. Crystallization was performed by the sitting drop vapor diffusion technique. The crystals of V_1-ATPase appeared under conditions using Ammonium Sulfate and Dioxane as precipitants. The optimized crystallization condition is as follows; 2-4 μl of a solution mixture of 20 mg/ml protein in a buffer solution of 10 mM Tris-Cl, pH 8.0, and the same volume of a reservoir solution were equilibrated against 500 μl of the reservoir at 293 K for 2 weeks. The reservoir solution consisted of 1.7 M Ammonium Sulfate, 10% (w/v) Dioxane, and 100 mM MES-NaOH, pH 6.0. Well-shaped hexagonal crystals with dimensions of $0.7 \times 0.5 \times 0.5$ mm^3 were obtained. Crystals were sealed in thin glass capillaries.

X-ray diffraction studies were performed at room temperature at the Photon Factory (BL6A and BL18B). Diffractions from these crystals extend to 6.0 Å resolutions. The data were processed using program HKL2000. These crystals belong to the space group $P321$ (or $P3_121$, $P3_221$). The unit cell dimensions were determined as a = 389.9 Å and c = 156.9 Å. Assuming that asymmetric unit contains two, three or four molecules of V_1-ATPase, the V_M value is calculated as 4.2, 2.8 or 2.1 Å^3/Da, respectively.

References

[1] K. Yokoyama, T. Oshima, and M. Yoshida, J. Biol. Chem. 265, 21946-21950 (1990).

* miki@kuchem.kyoto-u.ac.jp

6A, 6B/2000G131

X-ray crystallographic studies of prenyl transferases

Masahiro FUJIHASHI[1], Yuan-Wei ZHANG[2], Yoshiki HIGUCHI[1], Xiao-Yuan LI[2], Tanetoshi KOYAMA[2] and Kunio MIKI*[1,3]
[1]Department of Chemistry, Graduate School of Science, Kyoto University, Sakyo-ku, Kyoto 606-8502, Japan
[2]Institute for Chemical Reaction Science, Tohoku University, Katahira 2-1-1, Aoba-ku, Sendai 980-8577, Japan
[3]RIKEN Harima Institute / SPring-8, Koto 1-1-1, Mikazukicho, Sayo-gun, Hyogo 679-5148, Japan

Introduction

Over 23,000 structurally diverse isoprenoids are produced in nature, most of which are essential components of cellular machinery and serve as visual pigments, reproductive hormones, defensive agents, constituents of membranes and signal transduction components. Prenyltransferases, so-called prenyl diphosphate synthases, catalyze the prenyl chain elongation of prenyl diphosphates that are the common precursors of the carbon skeletons for all isoprenoids. These enzymes can be classified into two major sub-groups according to the *cis*- and *trans*-isomerism of products in the prenyl chain elongation.

Undecaprenyl diphosphate synthase (UPS) catalyzes the *cis*-prenyl chain elongation onto *trans, trans*-farnesyl diphosphate (FPP) to produce undecaprenyl diphosphate (UPP), which is indispensable for the biosynthesis of bacterial cell walls. We report here the crystal structure of UPS from *M. luteus* B-P 26 as the first three dimensional structure in all *cis*-prenyl chain elongating enzymes, in order to understand the molecular mechanism of *cis*-prenyltransferases.

Materials and Method

UPS from *M. luteus* B-P 26 was overproduced, purified and crystallized as described [1]. Heavy atom derivatives were prepared by the soaking method. For both thimerosal and $KAu(CN)_2$ derivatives, the concentration of heavy atom compounds in the soaking buffer and the soaking periods were 1 mM and 1 day, respectively. Diffraction studies were performed at room temperature at the Photon Factory (BL6A and BL6B).

Results and Discussion

The overall structure of UPS from *M. luteus* B-P 26 was determined at 2.2 Å resolution by multiple isomorphous replacement with anomalous scattering (MIRAS) [2]. This enzyme acts as a homodimer of 29 kDa subunits under physiological conditions. The asymmetric unit contains one homodimer, in which each monomer is crystallographically independent. The front view of the dimeric form of UPS looks like the face of an elephant. The contact interface of the dimer is about 15 %. The topology diagram of the secondary structures shows that the monomer has six parallel β-strands (S1-S6) and seven α-helices (H1, H2, H3, H5, H6, H8 and H10). The β-strands form a central β-sheet core, which is surrounded by five of the seven β-helices (H1, H2, H3, H5 and H10). Additionally, there are three short 3_{10}-helices (H4, H7, and H9) in each monomer.

The fold of UPS is completely different from those of other isoprenoid biosynthesis-related enzymes. These enzymes, including franesyl diphosphate synthases, pentalenene synthases, 5-epi-aristolochene synthases, squalene cyclase and protein farnesyltransferase, have a common structural motif. This motif is called the isoprenoid synthase (or terpenoids synthase) fold, and has been believed to be included in all enzymes related to isoprenoid biosynthesis. It is composed of 10 to 12 mostly antiparallel α-helices. However, UPS of the present study has a central β-sheet core, which is a different from the "isoprenoid synthase fold." Additionally, it was found that UPS belongs to a new protein folding family, judging from the multiple alignment of 3D structural neighbours search. This suggests that the catalytic mechanisms of UPS, including substrate recognition, are also different from those of other enzymes related to isoprenoid biosynthesis. Conserved amino acid residues among *cis*-prenyl chain elongating enzymes are located around a large hydrophobic cleft in the UPS structure. A structural P-loop motif, which frequently appears in the various kinds of phosphate binding site, is found at the entrance of this cleft. The catalytic site is determined on the basis of these structural features and the reaction mechanism to synthesize the C_{55} prenyl chain product is proposed.

References

[1] M. Fujihashi, N. Shimizu, Y.-W. Zhang, T. Koyama, and K. Miki, Acta Crystallogr., **D55**, 1606-1607 (1999).
[2] M. Fujihashi, Y.-W. Zhang, Y. Higuchi, X.-Y. Li, T. Koyama, and K. Miki, Proc. Natl. Acad. Sci. USA, **98**, 4337-4342 (2001).

* miki@kuchem.kyoto-u.ac.jp

6A, 18B/2000G140

The relationship between crystal structure and compressibility of DHFR mutants

Katsuo KATAYANAGI*, Yasunori KAMIYA, Masaki KAWAMOTO,
Takehiro SATO, Eiji OHMAE, Kunihiko GEKKO
Department of Mathematical and Life Sciences, Graduate School of Science, Hiroshima University,
Higashi-Hiroshima 739-8526, Japan

Introduction

As well as its 3D structure, the flexibility of protein molecule plays an important role in its function. Although structure-function relationships of enzymes have been widely investigated, it seems difficult to predict precisely the effects of amino acid replacements on the stability and function. Thus, we are now studying the structure-flexibility-function relationships of *Escherichia coli* dihydrofolate reductase (DHFR), which has four flexible loops. The flexibility of the whole molecule can be characterized by measuring the compressibility. From this criterion, DHFR is classified as "soft" protein and is suitable for the present study.

Results and Discussion

As we have already reported, we, at first, focused on the loop around the site 67 for the study of flexibility. This site was selected because position 67, being 29.5 Å away from the active site Asp27, is most flexible in a loop (residue 64-72) as revealed by large B-factor of the wild-type structure. We could find out the clear and linear correlation between the total volume of cavity from X-ray structure and compressibility.

Next, we focused on site 121, which is 19 Å away from active site. In both case of 67 and 121 site mutants, the large difference of distribution of the cavities between the wild-type and DHFR mutants was observed. The fact that these changes in cavities distributed all over the molecule suggests that the mutations at this position, being located in the surface loop, affect the structural dynamics and function of this enzyme by the long-distance effects as found by the double mutation experiments.

Comparing to loops at sites 67 and 121, the loop around site 145 is quite different. According to the results of double mutant study, the "long range interaction" was not observed between the sites of 67 and 145. Thus, we crystallized the DHFR mutants of A145X. The following table indicates all the mutants, which we have collected during current and previous proposal number.

G67 → A, V, L, S, T, D, C
G121 → A, D, F, Y, H, F, C
A145 → L, G, S, R, H, I

The data of compressibility experiments were already collected for these mutants. The crystals were obtained as a folate binary complex by vapour diffusion method at 4°C. The diffraction data, up to 2.1 Å resolution, were collected using beam line BL18B and BL 6B at Photon Factory. The crystal belonged to the space group $P6_1$ with lattice parameters a=93.0Å c=74.4Å. The initial phase was determined by the molecular replacement method. Then the crystallographic refinement was carried out using a program X-PLOR. As for the site 145 mutants, the structural analysis is now in progress. Then, we are planning to compare the distribution of the cavities between the wild-type and DHFR mutants, using the probe radius of 0.8 Å.

The crystal of DHFR mutants were not so stable during capillary mounting or cryo-mounting. The large number of crystals (about 10crystals) had to be tried to obtain a good diffraction dataset. This may be due to the fact that DHFR belongs the soft protein. The factor of "long distance interaction" will be identified through the viewpoint of detail 3D structure combined with double mutant analysis and the result of compressibility.

References

[1] Gekko,K., Kamiyama,T., Ohmae,E. & Katayanagi, K. *J. Biochem.*, **128**, 21-27 (2000).

* kkata@sci.hiroshima-u.ac.jp

15A/2000G146

Difference of acyl chain length of GM3 affects phase behaviors of binary mixtures of GM3 and DPPC

Sinzi MATUOKA*, Hirokuni YAMADA and Morio AKIYAMA
Sapporo Medical University, S.1 W.17, Chuo-ku, Sapporo, Hokkaido 060-8556, Japan

Introduction

We have been reported phase behavior of binary mixtures of 1,2-dipalmitoyl-L-phosphatidylcholine (DPPC) and native ganglioside GM3 prepared from equine red blood cells. In this report, we observed phase behaviors of binary mixtures of DPPC and GM3 with a C18:1 sphingoid base and a 24:0 acyl chain (GM3(18,24)) and those of DPPC and GM3 with a 18:0 acyl chain (GM3(18,18)) by x-ray diffraction(see Fig.1). The former GM3 is one of the major components of equine GM3. The latter has chain length similar to that of DPPC and is comparably minor component in equine GM3. By comparing phase behaviors of these two system, we investigated the effect of acyl chain length of GM3 on phase behaviors in binary mixtures of DPPC and GM3.

Materials and Methods

Ganglioside GM3(18,24) and GM3(18,18) was purchased from Wako Pure Chemical Industries, Ltd. (Osaka, Japan). DPPC was purchased from Avanti Polar Lipids, Inc. (Birmingham, AL). Mixtures of GM3 and DPPC dissolved in chloroform-methanol were dried under vacuum and then were hydrated with phophate buffer at 55 ℃ to prepare multilamellar vesicles.

X-ray diffraction measurements were carried out at BL-15A. The diffraction patterns were detected by imaging plates (Type BAS-III, Fuji Photo Film Co., Ltd., Japan).

Results

X-ray diffraction profiles of binary mixtures of GM3(18,24) and DPPC exhibited coexistence of two lamellar structure from 3 mol% to 7 mol% as shown in Fig.2a. This indicates that the formation of GM3-rich phase took place above 3 mol% and coexisted with GM3-poor phase from 3 mol% to 7 mol% and became dominant above 10 mol%. In GM3(18,18) / DPPC system, only the single lamellar structures were seemingly observed at least below 18mol% GM3 content (see Fig. 2b). However, lamellar repeat distance as a function of GM3(18,18) content (Fig.3) showed biphasic indicating formation of another phase which will be the GM3-rich phase. If this is the case, GM3-rich phase became dominant above 6 mol% GM3(18,18), which was different from the case of GM3(18,24).

The formation of GM3-rich phase will relate to biological functions such as cell adhesion and reactivity of antibody. It may be possible that cells regulate biological functions by varying acyl chain component of GM3 in the plasma membranes.

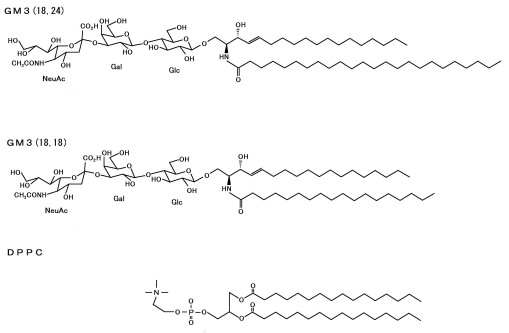

Fig. 1 Structures of GM3(18,24), GM3(18,18) and DPPC.

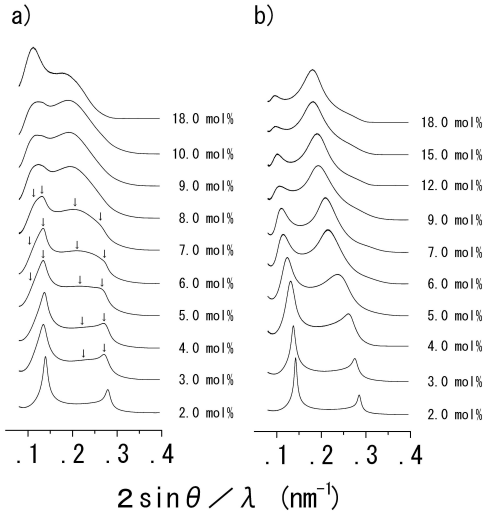

Fig. 2 X-ray diffraction profiles of binary mixtures of DPPC containing different molar ratios of a) GM3(18,24) and b) GM3(18,24) in the L$_\beta$ phase. Arrows represent peaks due to the lamellar repeats in coexistence region.

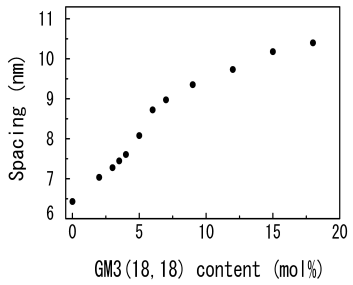

Fig. 3 Lamellar repeat distance as a function of GM3(18,18) content in the L$_\beta$ phase.

*matuoka@sapmed.ac.jp

10C/2000G152

Structural study of ferritin iron core by a combination of anomalous X-ray scattering and contrast variation techniques

Yoji INOKO*[1], Yasushi WATANABE[2], Katsumi KOBAYASHI[3]
[1] Division of Biophysical Engineering, Graduated School of Engineering Science, Osaka University, Toyonaka, Osaka 560-8531, Japan
[2]National Food Research Institute, Tsukuba, Ibaraki 305-8642, Japan
[3] KEK-PF, Tsukuba, Ibaraki 305-0801, Japan

Introduction

Ferritin is an iron-storage protein and its 24 subunits form a roughly spherical protein shell providing a cavity in which up to 4500 iron atoms are stored as a hydrous ferric oxide. We have been studying the structure of intermediate states of iron core formed during iron uptake by apoferritin using a technique of anomalous small-angle X-ray scattering (SAXS) [1-3]. The anomalous SAXS data has provided the size of growing iron core for iron-rich ferritin, but has not been able to determine accuracy core size for low iron-content ones since the contribution of anomalous scattering intensity from iron atoms to total intensity is relatively small. In this project, a contrast variation technique has been combined with anomalous scattering measurement to eliminate the obstructive scattering coming from the protein shell.

Experimental

SAXS experiments were carried out on the solution X-ray scattering camera at tunable beamline BL-10C at a wavelength of 1.488A for normal scattering measurements and various wavelengths near the ferric iron K-absorption edge (1.741A)[1]for anomalous scattering measurements. Scattering patterns were recorded by using a PSPC with an efficient detection length of 180mm. Intermediates were prepared by incubating apoferritin (horse spleen) and ferrous ammonium sulfate at various mole ratios and the actual iron content of reconstituted ferritin was determined spectrophotometrically.

Results and Discussion

In order to obtain the mean scattering density of the protein shell, the zero-angle scattering intensities from apoferritin were measured in 0.1M Hepes buffer containing different amount of sucrose in the range of 0 to 45 wt%. Figure 1 shows a plot of the square-root of zero-angle intensities derived from small angle scattering curves of various sample solutions against sucrose concentration. The zero intensity intercept of the regression line reveals that the zero contrast between the mean scattering densities of the solvent and protein shell is attained at 60 wt% sucrose, corresponding to an electron density of about $0.42e^-/A^3$. This value of mean scattering density obtained for apoferritin is significantly higher than those ($0.39\text{-}0.40e^-/A^3$) reported for most of other globular proteins.

Reconstituted ferritin containing different iron content have been studied in buffered 60 wt% sucrose solutions at which the scattering of the protein shell of ferritin approximately vanishes in the small angle region. The scattering measurements were done firstly at a wavelength of 1.488A to evaluate the core size of iron atoms deposited in various intermediate ferritin molecules by the Guinier analysis of their small angle scattering data. The apparent radius of gyration of iron core gradually

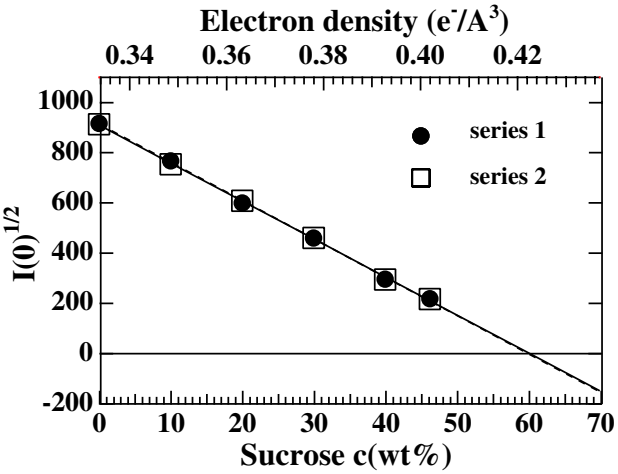

Figure 1. The square-root of zero angle intensities of horse spleen apoferritin solutions(0.076mg/ml) are plotted *versus* the electron density (top axis) and concentration (bottom axis) of the sucrose solvent.

increases from about 20A for 500 iron atoms/protein to about 28A for 3000 iron atoms/protein.

Next, the scattering intensity from various intermediate in 60 wt% sucrose solutions was recorded at wavelengths in the vicinity of the K-edge (1.741A) of ferric iron. The anomalous scattering part due to iron atoms was decomposed from a set of the total scattering profile measured at different wavelengths. The distribution of ferric iron atoms is to be calculated and compared with the size of the iron core obtained directly from the zero contrast measurements as described above.

References

[1] Y. Inoko et al., PF Activity Rep.**12**, 219(1994)
[2] Y. Inoko et al., PF Activity Rep.**15**, 55(1997)
[3] Y. Inoko et al., PF Activity Rep.**16**, 237(1998)

* inoko@bpe.es.osaka-u.ac.jp

15A/2000G154

Structure change of a molluscan smooth muscle during catch contraction

Yoshiko TAJIMA*[1], Akihiko ITO[1], Kouji MAKINO[2], Katsuzo WAKABAYASHI[3], Yoshiyuki AMEMIYA[4]

[1]Department of Physics,Tokyo Metropolitan University, Hachioji, Tokyo 192-0397, Japan

[2]The Institute of Physical and Chemical Research (Riken), Harima Institute at Spring 8, Hyogo 679-5143, Japan

[3]Division of Biophysical Engineering, Graduate School of Engineering Science, Osaka University, Toyonaka, Osaka 560-0043, Japan

[4]Department of Applied Physics, Faculty of Engineering, University of Tokyo, Bunkyo, Tokyo 113-8656, Japan

Introduction

Molluscan smooth muscles have a property of maintaining tension for a very long time with very little expenditure of energy (catch). Comparing between the small-angle X-ray diffraction patterns from the anterior byssus retractor muscle of *Mytilus edulis* (ABRM) in the early stage of catch and in the active state during phasic contraction [1], it was found that although the tension was lower in the catch state than in the active state, the axial periods of the thick filament reflections were larger in the catch state than in the active state [2]. It was confirmed in this work that the thick filaments were really elongated with transition of the ABRM from the active to the catch by comparing small angle X-ray diffraction patterns in the active state with those in the catch state which was produced just after recording the pattern of the active state.

Experimental Results and Discussions

Small-angle X-ray diffraction patterns were recorded on imaging plates using a point focusing camera with a camera-length of 170 cm. The ABRM was isometrically contracted by stimulation with acetylcholine (Ach). In order to detect spacing changes without missing a slight change much less than 0.1 %, high tensions were produced using a strong Ach solution (10^{-3} M) [3]. The pattern in the active state was recorded at a plateau of tension during stimulation with Ach solution which was flowed through the sample cell. The specimen was successively changed into the catch state by replacing the Ach solution with artificial sea water, and the X-ray pattern in the catch state was recorded 8 min after the replacement of the solutions when the ABRM was almost completely changed into the catch state. Then, the catch tension was relaxed by serotonin solution (2.5×10^{-5} M) to record the pattern in the resting state.

The intensities of the reflections from the thick and thin filaments were integrated radially. After subtraction of the background intensity, the profiles of the integrated intensity were compared between the resting, active, and catch states. The speed of relaxation of tension after replacing of Ach solution with artificial sea water depends on samples. If the amount of relaxation of tension 8 min after the replacement of the solutions is less than 25 % of the tension just before the replacement of the solutions, the axial periods of thick filament reflections are more elongated in the catch state than in the active state, contrary to the axial periods of the thin filament reflections which are decreased in the catch state (Table 1).

Table 1: Change in the axial periods of the meridional thick filament reflections and the thin filament layer line reflections compared with those in the resting state.

	Thick filament		Thin Filament	
	145 A	73	59 A	51
Active	0.25 %	0.25	0.76 %	1.09
Catch	0.34	0.28	0.59	0.49

Probably the thin filaments in the catch state play a role to tie the thick filaments by strong association between the myosin head and actin, and the tension is held by the thick filaments. The parts of thin filaments where myosin heads are not tied return to the structure of the resting state which is less extensible than the structure in the active state. Because the tension is transmitted to dense bodies, and the connective tissues by such thin filaments through the dense bodies joined to the cell membrane [4 & 5], the thick filaments are stretched by transition from the active state to the catch state in compensation for shrinkage of those thin filaments.

If the relaxation of tension is faster, the extension of the thick filaments in the catch state is probably cancelled out, and undetectable 8 min after washing of Ach.

References

[1] J. Lowy & B. M. Millman, Phil. Trans. Roy. Soc. B. 246, 105(1963).

[2] Y. Tajima, K. Makino, K. Wakabayashi & Y. Amemiya, PF Activity Report 18, 246(2000).

[3] Y. Tajima, K. Wakabayashi & Y. Amemiya, In *Synchrotron Radiation in the Biosciences*, ed. B. Chance, *et al.* pp. 509-518(1994).

[4] A. Sobieszek, J. Ultrastructure Research 43, 313(1973).

[5] B. M. Twarog, M. M. Dewey, & T. Hidaka, J. Gen. Physiol. 61, 207(1973).

* yoshiko@comp.metro-u.ac.jp

15A 2000G165

X-ray diffraction studies on the effect of reduction of stretch velocity in tetanized frog skeletal muscle by a CCD-X ray detector

Takakazu KOBAYASHI*[1], Hidehiro TANAKA[3], Katsuzo WAKABAYASHI[4], Yasunori TAKEZAWA[4], Yasunobu SUGIMOTO[4] and Haruo SUGI[2],
[1]Department of Electronic Engineering, Shibaura Institute of Technology, Minato-ku, Tokyo 108-8548
[2]Department of Physiology, School of Medicine, Teikyo Universuty, Itabashi-ku, Tokyo 173-8645
[3]Department of Physiology, School of Nursing, Teikyo Heisei Junior College, Ichihara, Chiba 290-0158
[4]Department of Biophysical Engineering, Graduate School of Engineering Science, Osaka University, Toyonaka, Osaka 560-8531

Introduction

When moderate stretch velocity is suddenly reduced during stretch in tetanized skeletal muscle, tension rises during the first part of stretch, and then starts to decay. To investigate molecular mechanism under-lying the stretch velocity sensitive force response to stretch, we measured the intensity changes of the meridional reflections of the X-ray diffraction with 15ms time resolution, which give information about behavior of actin-myosin linkages.

Materials and methods

The sartorius muscle fiber was mounted isometrically at in length and set to monochromatized X-ray beam path of wavelength 0.155nm from beam line 15A of synchrotron radiation. The muscle fiber was tetanized at 20Hz and then the muscle was stretched with moderate fast velocity (1.5%Lo, 0.15Lo/s) followed by slow (1.5%Lo, 0.015Lo/s) or opposite sequence during steady state of tension by the vibrator. The intensity of the meridional reflections was recorded by the CCD-Xray detector with tension. All experiments were made at 12℃.

Results

The intensity changes of 143 and 215 meridional refrection ($I_{143,}$ I_{215}) with fast stretch followed by slow and opposite sequence are shown Fig.1A and 1B. The I_{143} suddenly decrease during early phase of isometric tetanus and then recovered to lower level during steady state of isometric tetanus. The I_{143} further decreased during fast stretch and then slightly decreased during followed slow stretch (Fig. 1A). In contrast, the I_{143} slightly increased during slow stretch and then suddenly largely decreased during followed fast stretch (Fig. 1B). After completion of stretch the I_{143} recovered slowly to isometric tetanus level. The I_{215} decreased monotonically during rising phase of isometric tetanus and then no remarkable changed.

References

[1] H.Sugi : J.Physiol., **225**, pp 237-253 (1972)
[2] Y.Amemiya et al., J.Physiol., **407** pp231-241 (1988)
[3] T.Kobayashi et al., Biochem. Biophys. Res. Commun. **249**, 161-165 (1998)

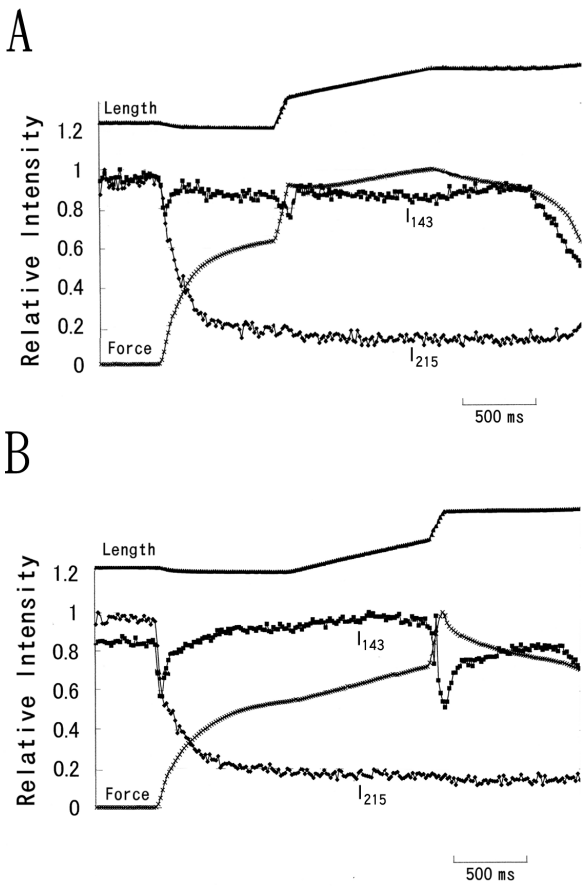

Figure 1. Length, force and intensity changes of 143 and 215 meridional reflection ($I_{143,}$ I_{215}) during fast stretch followed by slow stretch (A) and opposite sequence (B).

*kobataka@sic.shibaura-it.ac.jp

6A, 18B/2000G292

Structural analysis of bacterial transporter protein

Taiji Nakae*[1], Hiroyuki Akama[1], Atsushi Nakagawa[2], Tomitake Tsukihara[2]
[1]Tokai Univ., 143, Shimokasuya, Isehara, Kanagawa 259-1193, Japan
[2]Osaka Univ., 3-2, Yamadaoka, Suita, Osaka 565-0871, Japan

Introduction

The MexAB-OprM efflux pump of *Pseudomonas aeruginosa* exports xenobiotics including antibiotics out of cells contributing to multiantibiotic of this hospital pathogen. The pump assembly consists of the proton conducting transporter MexB[3], the membrane fusion protein MexA[1], and the outer membrane protein OprM[2].

An aim of this study is to obtain atomic level three-dimensional structure of these medically important and scientifically interesting transporter proteins and contribute for better understanding of multi- drug resistance.

Experiments and Results

We collected the data of native crystals using an ADSC detector and synchrotron radiation with 1 Å wavelength and 350mm distance at 95 Kelvin.

The data were processed using MOSFLM program package. OprM was belonging to rhombohedral space group R32 with unit cell parameters of a = b = 85.23 Å, c = 1042.66 Å. The crystals diffracted beyond 3.4 Å (Figure right), but we have been perplexed with anisotropic diffractional pattern. (Figure left)

Data collections and analysis of derivative crystals are now in progress.

References

[1] H. Yoneyama et al., J. Biol. Chem. Vol.275, No.7, pp. 4624-4638 (2000).
[2] A. Nakajima et al., J. Biol. Chem. Vol.275, No.39, pp. 30064-30068 (2000).
[3] L. Guan et al., J. Biol. Chem. Vol.274, No.15, pp. 10517 -10522 (1999).

*nakae@is.icc.u-tokai.ac.jp

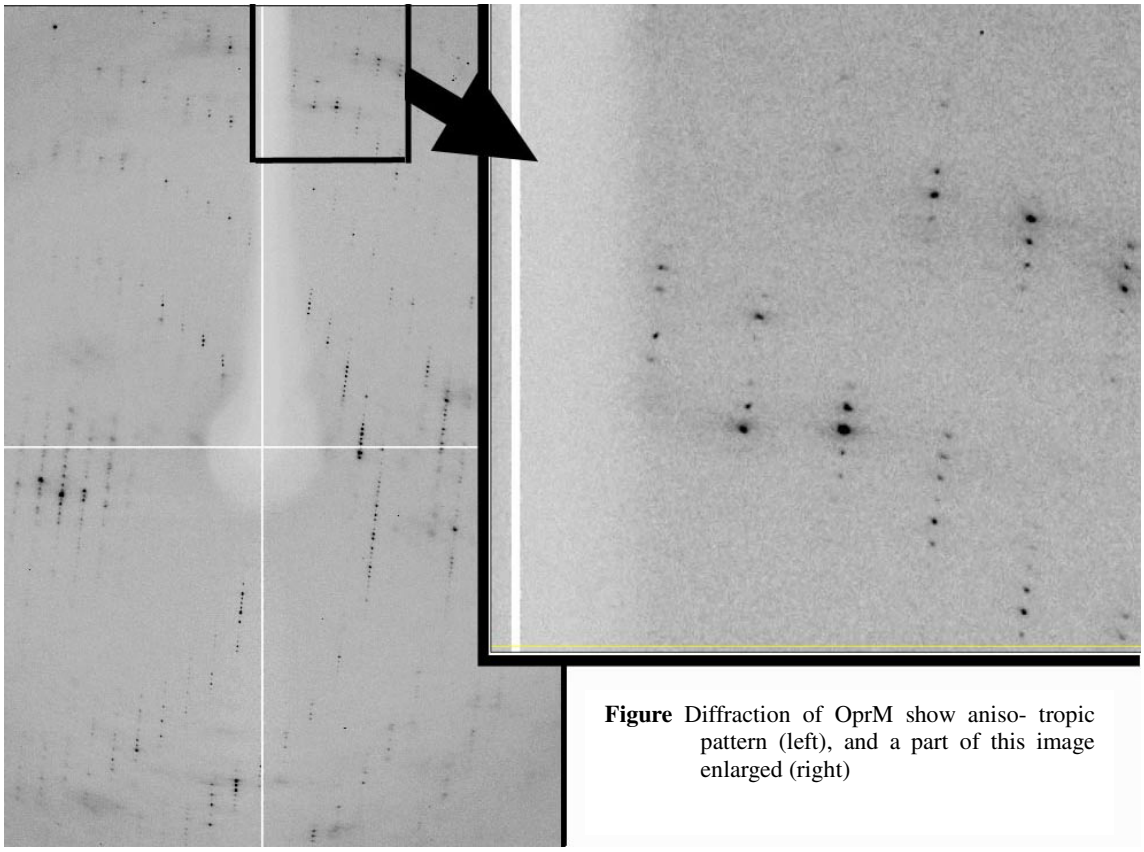

Figure Diffraction of OprM show aniso- tropic pattern (left), and a part of this image enlarged (right)

6A, 18B/2000G296

Rational drug designs based on crystal structures of the Hepatitis C Virus NS3 helicase-inhibitor complexes

Chih-Yung Hu[1], Shen-Jia Chen[1], Shwu-Huey Liaw*[123]
[1]Institute of Biochemistry, [2]Department of Life Science, National Yang-Ming University, and
[3]Department of Medical Research and Education, Taipei Veterans General Hospital, Taipei, Taiwan

Introduction

Hepatitis C virus (HCV), a positive-stranded RNA virus of the *Flaviviridae* family, is the major causative agent of transmitted non-A, non-B hepatitis and currently infects approximately 3% of the world's population. The infection easily results chronic hepatitis, and then may lead to liver cirrhosis and hepatocellular carcinoma. Unfortunately, no effective treatments for hepatitis C virus are available. Nonstructural protein 3 (NS3), one of the virus proteins, is a 631-residue bifunctional enzyme with the N-terminal 180-residue serine protease domain and the C-terminal 450-residue helicase domain. Here we report crystal structures of NS3 helicase domain from a Taiwanese HCV strain, complexed with various inhibitors, which would provide more knowledge in further rational drug design.

Materials and methods

To identify potential inhibitors for HCV helicase, the structural-based searches through available chemical databases were performed using the DOCK program. Following DOCK screening, more than ten potential inhibitors were selected and purchased for the enzymatic assay and structural studies. The NS3 helicase domain from a Taiwanese HCV strain was expressed, isolated, and crystallized as described previously. The crystals belong to the space group $P3_121$, with the unit cell dimensions of a = b = 92 Å, and c = 105 Å at the cryotemperature. The crystals soaked in various amounts of inhibitors for different length times, and the diffraction data were measured at 100 K. The crystal structures were solved by using the program AMORE in the CCP4 suite, and refined using *CNS* and *TURBO*.

Results and discussion

As the previously solved structures, the helicase domain consists of three structural domains forming a Y-shaped configuration [1]. Domains 1 and 2 have similar topologies, composed of a large central parallel β-sheet flanked by α -helices, whereas domain 3 is predominantly α-helical. In this study, the inhibitors bind at the interdomain cleft between domains 1 and 2.

The Fo – Fc density maps revealed that blue HT has the highest affinity to the enzyme among the inhibitors. In consistence with, the activity assay also showed that blue HT strongly inhibits the enzyme activity. The sulfate group interacts with five consecutive main chain NH groups of residues 207-211 (GSGKS), the side chain of Ser 211, and an additional water-mediated contact to Asp 290. The benzyl ring has close contact with Tyr 241 and Phe 238, and the amino group interacts with the backbone carbonyl group of G237 (Fig. 1).

In short, the negatively charged sulfonate group of blue HT contributes the major interaction, while the *para*-conformation avoids steric hindrance [2]. Further rational drug design could be performed by using the blue HT as a lead compound. Potential inhibitors containing the *para*-chain in blue HT will be searched through the databases, verified by the DOCK program, and selected for further characterization.

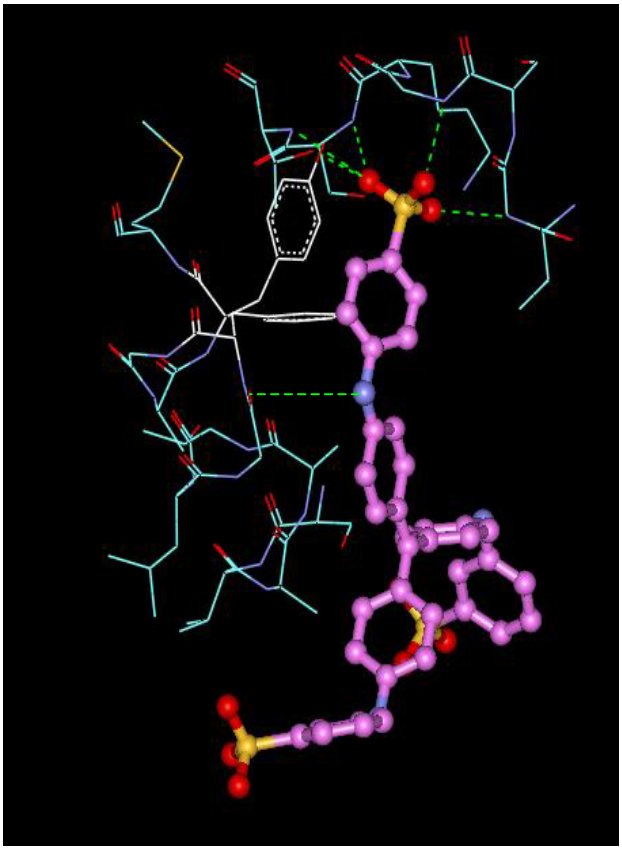

Fig. 1 The detailed interaction between BlueHT and NS3 helicase.

References

[1] J.L. Kim et al., *Structure* 6:89-100 (1998).
[2] S.-H. Liaw et al., in preparation.

* shliaw@ym.edu.tw

6A, 18B/2000G308

Three-dimensional structure of a nicotinoprotein formaldehyde dehydrogenase

Nobutada TANAKA*, Yoshio KUSAKABE, Hiroshi UEMURA, Masato KONDO,
Yasuyuki KITAGAWA, and Kazuo T. NAKAMURA
Laboratory of Physical Chemistry, School of Pharmaceutical Sciences, Showa University,
1-5-8 Hatanodai, Shinagawa-ku, Tokyo 142-8555, Japan

Introduction

Formaldehyde dehydrogenases (FDH; EC 1.2.1.1) have been found in a wide variety of organisms. These enzymes belong to the zinc-containing medium-chain alcohol dehydrogenase (ADH) family. Most FDHs are known to require NAD^+ and glutathione for the oxidation of formaldehyde. Formaldehyde dehydrogenase from *Pseudomonas putida* (PFDH; EC 1.2.1.46) is a unique enzyme that can catalyze NAD^+-dependent oxidation of formaldehyde without the external addition of glutathione. Since formaldehyde is a toxic compound, it is natural that most organisms have developed several oxidation systems to counteract this compound. The PFDH enzyme, in its active form, is a homotetramer of identical subunits, each of which comprises 398 amino acid residues and two zinc ions (the catalytic zinc and the structural zinc), and has a molecular mass of about 42 kDa. A comparison of amino acid sequences shows that PFDH belongs to the zinc-containing medium-chain ADH family, although there are extensive variations in the amino acid sequence. When PFDH is incubated with NAD^+ and either formaldehyde or acetaldehyde, NADH production can be detected as an increase in A_{340}, whereas no increase in A_{340} is observed with propanal or longer chain aldehydes. However, PFDH catalyzes the efficient dismutation of a wide range of aldehydes where two molecules of the aldehydes are converted to one molecule each of the corresponding carboxylate and alcohol.

A remarkable feature of PFDH, as compared with the ADHs, is that the enzyme is a nicotinoprotein. Nicotinoproteins are proteins that contain NAD(P)(H) as a tightly bound redox active cofactor. The NAD(P)(H) in these enzymes is tightly but not covalently bound to the enzyme and does not exchange with the cytosolic NAD(P)(H) pool in contrast to typical ADHs that use NAD(P)(H) as an exchangeable coenzyme (co-substrate). It is an interesting question whether there are common structural features among the nicotinoproteins, and if so, which features are responsible for the tightly bound NAD(P)(H) cofactor. Thus, the three-dimensional structure of PFDH is essential not only to clarify the mechanism of the glutathione-independent oxidation of formaldehyde, but also to reveal the structural origin of the tightly bound cofactor among the nicotinoprotein dehydrogenases.

Results and Discussion

The crystal structure of PFDH was determined by the multiwavelength anomalous diffraction (MAD) method using intrinsic zinc ions and refined to an R-factor of 0.171 (free R-factor of 0.206) at a 1.65 Å resolution [1]. The present model includes one NAD^+ molecule, two zinc ions and all of the non-hydrogen atoms except for the N-terminal (Ser1) and C-terminal (Ala398) residues for each of the two crystallographically independent subunits. In addition, a total of 967 water molecules and two sulfate ions are included per asymmetric unit (ASU). The geometry of the current model was such that the root-mean-square deviations (RMSDs) from ideal values are 0.009 Å for bond lengths and 0.025 Å for bond distances. According to a Ramachandran plot for the current model, a total of 586 (89.6 %) non-glycine and non-proline residues have their ϕ, ψ angles in the most favored region, whereas the remaining 68 (10.4 %) non-glycine and non-proline residues are in the additional allowed region.

The 170-kDa-homotetrameric PFDH molecule shows 222-point group symmetry. Although the secondary structure arrangement and the binding mode of catalytic and structural zinc ions in PFDH are similar to those of typical ADHs, a number of loop structures that differ between PFDH and ADHs in their lengths and conformations are observed. A comparison of the present structure of PFDH with that of horse liver ADH, a typical example of an ADH, reveals that a long insertion loop of PFDH shields the adenine part of the bound NAD^+ molecule from the solvent, and a tight hydrogen-bond network exists between the insertion loop and the adenine part of the cofactor, which is unique to PFDH. This insertion loop is completely conserved among the nicotinoprotein formaldehyde dehydrogenases, whereas it is replaced by a short turn among typical ADHs. Thus, the insertion loop specifically found among the nicotinoprotein formaldehyde dehydrogenases is responsible for the tight cofactor binding of these enzymes and explain why PFDH can effectively catalyze alternate oxidation and reduction of aldehydes without the release of cofactor molecule from the enzyme.

References

[1] N. Tanaka et al., submitted.

* ntanaka@pharm.showa-u.ac.jp

6A, 18B/2000G313

Crystal structures of two lectin isomers from the roots of pokeweed

Tomomi FUJII[1], Minoru HAYASHIDA[1], Masatsune ISHIGURO[2], Yasuo HATA*[1]
[1]Inst. for Chem. Res., Kyoto Univ., Gokasho, Uji, Kyoto 611-0011, Japan
[2]Dep. of Gen. Res. Tech., Fac. of Agr., Kyushu Univ., Fukuoka 812-8581, Japan

Introduction

Pokeweed lectin is a lectin specific for *N*-acetylglucosamine-containing saccharides, and stimulates peripheral lymphocytes to undergo mitosis by binding to their cell surfaces. Several lectins have been isolated from pokeweed roots and shown that they are homologous proteins but have different molecular sizes and biological properties [1]. They are composed of several chitin-binding domains homologous to wheat germ agglutinin. In these proteins, PL-Ds composed of two domains are the smallest one in the group and have two isomers, PL-D1 and PL-D2. PL-D1 consists of 84 amino acid residues (M_r = 9,317), while PL-D2 has an identical sequence with PL-D1 except lack of the C-terminal Leu83-Thr84 [2]. Both PL-Ds showed the agglutinating activity toward trypsin-treated erythrocytes. Although PL-D2 presents mitogen activity toward lymphocyte cell, PL-D1 does not. We determined the crystal structures of PL-D1 and PL-D2 in order to elucidate the structural basis for mitogen activity of pokeweed lectine.

Experimental

Crystals of PL-D2 was obtained by batch method using seeding technique with reservoir solution of 18% PEG8K, 0.2M Calcium acetate, and 0.1M Na acetate buffer pH4.6 at 25°C. Diffraction data for PL-D2 was collected on a screenless Weissenberg camera with imaging plates (400 mm 200 mm size) at the BL18B station of the Photon Factory. The data collection of PL-D2 was performed at 291K with two crystals with different orientation sealed in a glass capillary. The data were processed, scaled and merged with programs DENZO and SCALEPACK. The crystal belongs to space group $P2_1$ with unit cell dimensions of a = 23.24 Å, b = 56.95 Å, c = 29.62Å, β = 109.3° containing one molecule in the asymmetric unit.

The structure of PL-D2 was determined by molecular replacement method using program MOLREP of program suit CCP4. The fourth-domain of wheat germ agglutinin isolectin 3 was employed as a starting model. The refinement was carried out using programs X-PLOR and CNS. The refinement of the current model was converged to an *R*-factor of 17.6% and the free *R*-factor of 20.7% at 1.5 Å.

Crystals of PL-D1 were grown by a hanging drop vapor diffusion method with reservoir solution of 30% PEG8K, 0.2M Calcium acetate, and 0.1M Na phosphate buffer pH6.5 at 25°C. Diffraction data for PL-D1 was collected on an ADSC Quantum 4 CCD detector at the BL6A station of the Photon Factory. The data collection of PL-D1 was performed at 100K with a flash-cooled crystal in the liquid nitrogen gas stream. The data were processed, scaled and merged with program DPS/MOSFLM and CCP4 program suit. The crystal belongs to space group $P2_12_12$ with unit cell dimensions of a = 48.67 Å, b = 49.01 Å, c = 29.93 Å containing one molecule in the asymmetric unit.

The structure of PL-D1 was determined by molecular replacement method using program MOLREP of program suit CCP4 using PL-D2 model as a starting model. The refinement using program CNS was carried out. The refinement of the current model was converged to an *R*-factor of 17.5% and the free *R*-factor of 20.2% at 1.6 Å.

Results and Discussion

The polypeptide folds of PL-Ds consists of two hevein-type domains, which have no secondary structure. On the comparison with PL-D2, the inclination of the arrangement of the domains in PL-D1 is about 10°. These facts indicates that the flexibility between two domains in PL-Ds. In the crystal structure of PL-D2, calcium ion binds the C-terminal regions. The β-carboxyl group of Asp57, α-carboxyl group of Asp82, β-carboxyl group of Asp48 in neighboring molecule, and three water molecules coordinate to the ion. Although these interactions apparently participate in the formation of crystal lattice, the physiological meaning of these interactions is unknown.

The electron density of the excess elongating C-terminal region, Leu83 and Thr84, of PL-D1 is not observed in the present crystal. One simple hypothesis could be supposed that the region around C-terminus of PL-D2 is the binding site for target protein which would cause mitogen activation. The flexible elongated C-terminal two amino-acid residues of PL-D1 may prevent the interaction.

References

[1] M. Kino et al., Biosci. Biotech. Biochem. **59**, 683 (1995).
[2] K. Yamaguchi et al., Biosci. Biotech. Biochem. **60**, 1380 (1996).

*hata@scl.kyoto-u.ac.jp

12A/2000G327

Evaluation of a new magnetic type of X-PEEM

Keiji YADA[*1, 2], Minaji FURUDATE[1], Kunio SHINOHARA[3], Atsushi ITO[4], and Makoto WATANABE[1]
[1]IMRAM, Tohoku Univ., Sendai-shi, 980-8577, Japan
[2]Tohken Co Ltd., Chofu-shi, Tokyo 182-0025, Japan
[3]Graduate School of Medicine, Univ. of Tokyo, Bunkyo-ku, Tokyo 113-0033, Japan
[4]School of Engineering, Tokai Univ., Hiratsuka-shi, Kanagawa 259-1292, Japan

Introduction

We constructed a new magnetic type X-PEEM (X-ray photoemission electron microscope) which has a salient feature of wavelength-scan capability suitable for spectroscopic X-ray microscopy. This is especially effective in the case of elemental analysis of biological sample. High resolution, operational easiness and compactness were aimed as the basic design concept. Performance test as X-PEEM was carried out using light source from BL-12A at the PF after testing as the TEM and target-X-PEEM at Tohoku University.

Results and Discussion

Lenz paremeters of the objective of the X-PEEM are as follows: Cs = 8 mm, Cc = 7 mm, fo = 8 mm, accelerating potential for photocathode V = 15-16 kV. As the photocathode, thin gold film (30 nm thick) was used among tested several materials such as Au, CsI, CuI, MgF because of chemical stability. As the standard sample of resolution, diatomite having very small holes (0.2-0.3 μm in diameter) from Toyokuni Diatomite Industry Co., Oita, Japan was used. As a biological sample, critical point dried HeLa cells were prepared.

Figure 1 shows an example of the diatomite taken using 0th order X-ray beam with 100 μm objective aperture in comparison with SEM image of the corresponding field. It is seen that about 0.2 μm holes are rather clearly separated.

Figure 2 shows X-ray images of a HeLa cell taken at different wavelength. Image (b) taken with 24 Å X-rays is much clearer than image (a) taken with 0th order synchrotron light. It was proved that the microscope has wavelength-scan capability as expected in the range 11-35 Å and also stably operative during long and repeated exposures.

At the beginning of the present plan, resolution better than 100 nm was expected as X-PEEM but the practically attained resolution is about 200-300 nm, though the resolution when operated at TEM mode is about 30 nm. It seems that rather large energy spread in the photoelectron by X-ray irradiation plausibly causes large chromatic defect. Image filtering will be necessary in the future for better resolution.

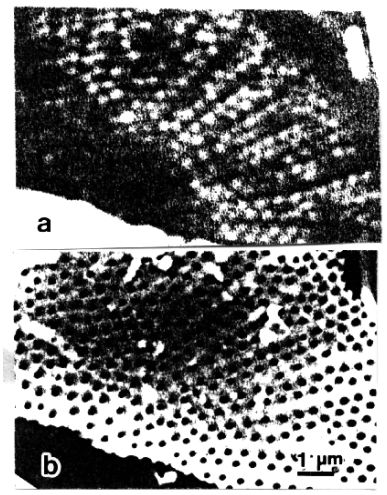

Fig. 1. X-ray image (a) and SEM image (b) of diatomite.

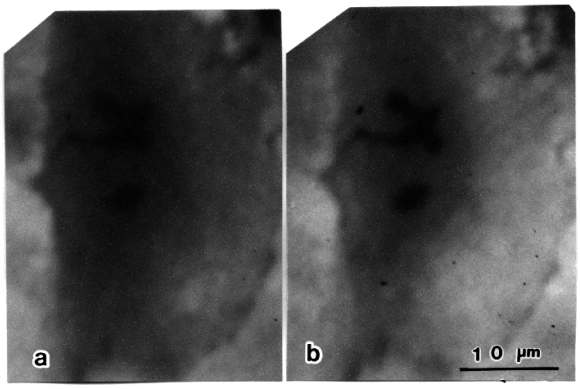

Fig. 2. HeLa cell taken with 0th order light (a) and with 24 Å light (b).

* kyada@tohken.co.jp

11B/2000G328

XANES of intracellular local areas in a human HeLa cell at the phosphorus K absorption edge

Atsushi ITO*[1], Hiroyuki MATSUDA[1], Yoshinori KITAJIMA[2], and Kunio SHINOHARA[3]
[1]School of Engineering, Tokai Univ., Hiratsuka-shi, Kanagawa 259-1292, Japan
[2]KEK-PF, Tsukuba, Ibaraki 305-0801, Japan
[3]Graduate School of Medicine, Univ. of Tokyo, Bunkyo-ku, Tokyo 113-0033, Japan

Introduction

XANES of biological specimens provides a unique method for molecular imaging using resonance absorption peaks assigned to a specific chemical bond with the aid of soft X-ray microscopy. DNA and its related compounds such as nucleotides have a sharp and intensive resonance peak at the phosphorus K absorption edge[1], suggesting the possibility of sensitive mapping of P-containing molecules. In the present study, we have obtained XANES of local regions with the area of 0.5 square microns in a human HeLa cell that were derived from a number of contact images around the P-K absorption edge. Furthermore, from these XANES spectra distribution of P-containing molecules was elucidated using a computer program that was developed for this purpose.

Materials and Methods

Contact X-ray microscopy using an electronic zooming tube was used to obtain X-ray images of human cancer HeLa cells that are subjected to critical point drying at the P-K absorption edge at the resolution about 0.5μm[2]. BL-11B beamline was used for this energy region. XANES of local areas in a HeLa cell were obtained from 13 X-ray images around the P-K edge including a XANES peak energy. From the ratio of absorption between at the peak energy and at the energy just below the peak for every pixel that constitute the images, distribution of P-containing molecules was obtained.

Results and Discussion

Figure 1 shows a group of HeLa cells taken at 2140eV. Small white areas of 0.5μm square were sites of XANES measurement. Absorption spectra for these areas were shown in Figure 2. XANES in the areas of 1, 2 and 3 exhibited the similar profile to that of DNA shown by the dotted line. In contrast spectra of area A and B, which locate outside the cells, exhibited rather broad structure. Figure 3 shows the result of DNA mapping of HeLa cells. This image indicates that DNA and P-containing molecules distribute throughout the cells with nearly uniform density. These cells appear to be densely packed, because optical microscopic observation showed dense and uniform morphology compared with other interphase cells. Further experiment is being planned in which spectra of nuclear and cytoplasmic region could be discriminated from the spectral profile.

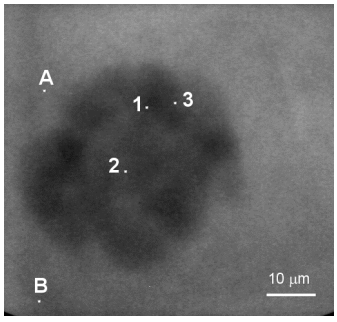

Fig. 1. Soft X-ray image of HeLa cells at 2140eV. Areas of 1, 2, 3, A and B with 0.5 square microns are the sites for XANES.

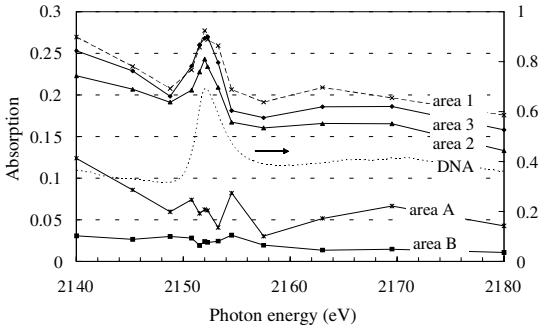

Fig. 2. XANES spectra of local areas in a HeLa cell at the P-K absorption edge. Dotted line shows a spectrum of calf thymus DNA.

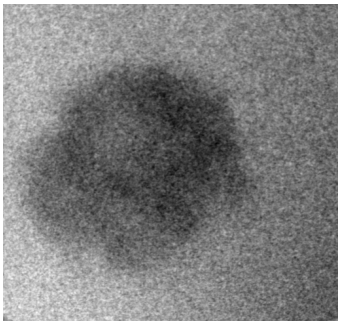

Fig. 3. Image of P-containing molecules in HeLa cells.

References

[1] A. Ito et al., In "X-RAY MICROSCOPY", (ed. by W. Meyer-Ilse et al.), pp. 145-148, New York, AIP (2000).
[2] K. Shinohara et al., In "X-Ray Microscopy and Spectromicroscopy", (ed. by J. Thieme et al.), pp. I-169~I-173, Heidelberg: Springer, (1998).

* aeito@keyaki.cc.u-tokai.ac.jp

27A/2000G329

Lethal effect of k-shell photoionization of phosphorus on radiosensitive cell lines

Kiyomi EGUCHI-KASAI*[1], Hiroshi MAEZAWA[2], Koki SATO[3], Katsumi KOBAYASHI[1]
[1]Radiat. Hazards Res. Gr., NIRS, Chiba, Chiba 263-8555, Japan
[2]Sch. of Health Sci., The Univ. of Tokushima, Tokushima, Tokushima 770-8509, Japan
[3]The Sch. of Biol.-Oriented Sci. & Technol., Kinki Univ., Naka-gun, Wakayama 649-6493, Japan
[4]KEK-PF, Tsukuba, Ibaraki 305-0801, Japan

Introduction

DNA is considered to be the critical target for cell killing by ionizing radiation. Therefore it is expected that the photoionization of phosphorus in DNA may cause some specific biological effects[1].

Many radiosensitive mammalian mutant cell lines have been established in these 40 years. They lack at least one gene which is involved in DNA repair system. By the complementation test, these cell lines are classified into at least 9 groups. Most of these genes have already been cloned in these several years. The usage of these mutants should help to clarify the nature of DNA damage.

These facts prompted us to test the lethality caused by k-shell photoionization of phosphorus in some radiosensitive mutant cell lines. We already reported the lethality of 2 mutant cell lines (SX9 is grouped as XRCC7 which is defective in DNA-PKcs and SX10 defective in DNA ligase IV) and 1 wild cell line (FM3A which is the wild type parents of SX9 and SX10) [2]. This year, we will report the results for other radiosensitive cell lines of irs1 and irs1SF.

Materials and Methods

Cells

Two Radiosensitive mutant cell lines of irs1 (XRCC2) and irs1SF (XRCC3) were used. These genes are the important components of homologous recombination which is on of the pathway of the DNA double strand break repair. Cells were cultured in plastic culture bottles with alpha-MEM medium with 10% fetal bovine serum and antibiotics.

Exposure

Monochromatic X-rays at 2.153 keV (K-shell resonance absorption peak of phosphorus), 2.146 keV and 2.160 keV (off peak) were selected for irradiation by an InSb double-crystal monochromater at BL-27A. A plastic dish, in which exponentially growing cells were attached, was set on a sample scanning stage to make uniform irradiation with X-rays. After irradiation, cells were plated in appropriate number and cultured for the colony formation.

Results and Discussions

Survival curves of irs1 andirs1SF cells after x-rays irradiation were shown in Fig.1. Linear-quadratic survival curves were obtained for three energies. Lethal effect at 2.153 keV and 2.160 keV was larger than that at 2.146 keV in both cell lines. Lethal enhancement ratio (LE), which was defined as the ratio of 10% survival dose at 2.153 keV and 2.160 keV to that at 2.146 keV, was 1.6 and 1.1, respectively, for both cell lines. LE values were very similar to the wild-type SR-1 cells reported previously[2].

Studies on lethal effects are now going on different radiosensitive mutants those are defective in other DNA repair pathway(s).

Fig.1 Survival curves of irs1 and irs1SF cells. One R corresponds to 2.58 x 10^{-4} C/Kg.

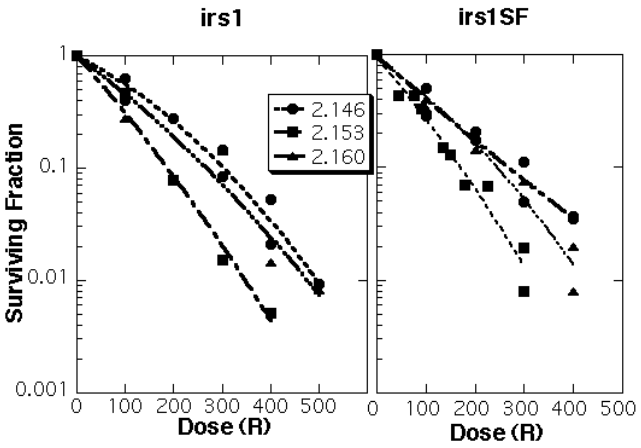

References

[1] J.L. Humm, KFA Report JUL-1932 Kernforschungsanlage, Jurich, 10(1984).
[2] K. Eguchi-Kasai *et al.*, Photon Factory Activity Report 2000, **18**, 258(2001).
[3] H. Maezawa *et al.*, Photon Factory Activity Report 1999, **17**, 271(2000).

* kiyomiek@nirs.go.jp

15A1/ 2000G330

Formation of a compact structured ensemble early during ubiquitin folding investigated by stopped-flow CD, x-ray scattering and fluorescence

Zhijie QIN,[1] John ERVIN,[2] Edgar LARIOS[2], Martin GRUEBELE,[2] Hiroshi KIHARA*[1]
[1]Department of Physics, Kansai Medical University, Hirakata 573-1136, Japan
[2]Department of Chemistry, Univ. of Illinois at Urbana-Champaign, IL 61801, USA

As is β-lactoglobulin, we found ubiquitin, one of the smallest predominantly β-sheet proteins, also collapses first to a compact but not tightly packed state with excess helical structure.

Ubiquitin, used in the present experiments was Phe45Trp-mutated to have a tryptophan as a probe (abbreviated as Ub*).

The current work investigates the early stages of ubiquitin folding in viscous solvents and at low temperatures (T = 4 °C and –20 °C). Ethylene glycol (EtGOH, 45 %) was added as an antifreeze.

The X-ray scattering measurements were taken at beamline 15A1. The X-ray wavelength was λ =1.50 Å with either PSPC or CCD.

Results and discussion

The results for the non-equilibrium measurements at –20 °C are shown in Fig. 1. There are three phases present at both temperatures. At –20 °C, a fast phase can be seen within the dead time (6 ms) of the apparatus in panels A and C. The fluorescence signal has minimal amplitude for the fast phase, but it does show the two slower phases clearly. The slowest phase can be seen in both fluorescence and circular dichroism data; it cannot be resolved in the X-ray scattering data due to its lower signal-to-noise-ratio. The 4 °C X-ray data (not shown) shows a burst phase as well. Again the fluorescence is insensitive to this burst phase.

The CD value of the burst phase intermediate indicates greater-than-native helix content in the burst phase intermediate. This increase in helix goes hand in hand with a large reduction in the radius of gyration of the protein, as can be seen in Fig. 1 where R_g of the protein decreases by 6Å in < 6 ms. At 4 °C the CD signal also shows a rapid decrease (data not shown) but no phases after the initial rapid decrease are resolved. The R_g at this temperature decreases by 9Å within 6 ms.

Figure 1: Ub*, –20° refolding in 45% EtGOH. The refolding was followed by CD at 222 nm (**A**), 295 nm excited fluorescence integrated above 335 nm (**B**), and R_g (**C**). The three data sets were fit to a double exponential decay as described in the text. The fit is shown as a solid line through the points.

*kihara@makino.kmu.ac.jp

6A, 18B/2000P020

Structure analysis of artificial proteins

Tsuyoshi Shirai[*1]
Nagoya University, Furo-cho, Chikusa-ku, Nagoya, 464-8603 Japan

Introduction

Periodicities are the recurring theme observed in structures of proteins, genes, and genomes. Reiteration of short DNA sequences has been thought to gave birth to rudimentary biological structures in proteins. In this study, the structures of three artificial proteins encoded by artificially reiterated short DNA sequences and created periodic DNAs that have long open reading frames (microgene polymer proteins) were investigated by using SR light source.

Results

SAXS experiments

To know whether artificial proteins fold as compact as natural protein does, small angle X-ray scattering (SAXS) analyses was performed with solution of the three microgene polymer proteins, namely, #287 (Cu^+), #292 (Cu^+) and #320 (α^+).

SAXS experiment was carried out at the solution scattering station installed at BL-10C, Photon Factory. Proteins were dissolved in 10 mM phosphate buffer containing 0.1 M NaCl (pH 6.0) and placed in a cell (1 mm X-ray path length with 20 m thick quartz windows) for the measurements. Wavelength of incident X-ray was 1.488 Å and the size of beam cross-section was 0.5 × 3.0 mm^2. The sample to detector distance was 202 cm, calibrated with meridional diffraction of dried chicken collagen. The same solution without protein was measured as background. The measurements were executed at an ambient temperature.

The SAXS data have revealed that the radii of gyration (Rg) of #287 (Cu^+), #292 (Cu^+) and #320 (α^+) were 29.0Å, 26.6Å and 26.6Å based on the calculations of Guinier plot. These values were compared with the radius of gyration of natural proteins in their native form and in their denatured form. If #320 protein, whose molecular weight is 12,306, exists as monodisperse molecule in the solution, the data suggested the protein adopt molten state. In agreement with this conclusion, the molecular weight of #320 protein in gel filtration experiments with and without denaturant were calculated as about 50K. The Krutky plot of the small angle X-ray scattering data suggested the protein has globular structure rather than elongated structure.

Powder diffraction experiments

The results from small-angle X-ray scattering analyses suggested that some of the microgene polymer proteins would take a unique and compact conformation under a certain condition.

This possibility was inquired by screening for crystallization conditions for the proteins. The #320 (α^+), #292 (Cu^+) and #287 (Cu^+) proteins were used for crystallization experiments with the reagents and methods usually applied for natural proteins. As a result, a protein crystal was obtained for #320 (α^+).

The protein was crystallized by using the hanging-drop vapor-diffusion method. A 50 mM HEPES buffer (pH 6.5) containing 25% (w/v) PEG-4000 and 20% (v/v) glycerol was used for a reservoir (1 ml). A drop containing a 5 µl of 1% (w/v) protein solution in 50 mM phosphate buffer and a 5 µl of the reservoir solution was equilibrate against the reservoir. A lot of micro-crystals appeared in few days at a room temperature. The largest crystal had a dimensions of ~0.2 × 0.2 × 0.01 mm^3. The crystals were rinsed with the reservoir solution and were confirmed that they are composed of #320 (α^+)by a SDS-PAGE.

The micro-crystals were scooped up with a cryo-loop (Hampton research) from a hanging drop and flush-frozen in a liquid nitrogen. X-ray diffraction experiment was carried out at BL-18B station, Photon Factory. (λ = 1.00 Å). The frozen drop was kept in a 100 K nitrogen stream from a cryo-system (Oxford Cryosystem) during the experiment. The diffraction image was recoded for 10 min. by using CCD detector.

Although the #320 (α^+) crystal did not diffract well, a powder diffraction-like pattern was observed after a long time X-ray exposure. From the observed three distinct diffractions, two possibilities remained that the unit cell is 3D with dimensions (a, b, c) = (30, 18, 15 A^3) or it is 2D crystal with dimensions (a, b) = (30, 18 A^2). In either case, the crystal has proved that the microgene polymer protein can generate a ordered structure in condition dependent manner.

References

[1] K. Siba, Y. Takahashi & T. Noda, J. Mol. Biol., *in press* (2002).

*i45282a@nucc.cc.nagoya-u.ac.jp

14B, 15C/2001G053

X-ray optics for observing dark-field and bright-field refraction-contrast images

Keiichi HIRANO*, Anton MAKSIMENKO, Hiroshi SUGIYAMA and Masami ANDO
KEK-PF, Tsukuba, Ibaraki 305-0801, Japan

Introduction

Because X-ray refraction-contrast imaging by means of a crystal analyzer has a much higher sensitivity to light elements (Z<17) than conventional X-ray imaging techniques based on absorption, it is very useful for observing the inner structures of biological and polymeric objects. Here we report on a new X-ray optics using a Bragg-transmission analyzer for observing both dark-field and bright-field refraction-contrast images [1].

Experimental and results

Our optics consists of a collimator and an analyzer in the Bragg geometry as shown in Fig. 1. Both optical elements are prepared from perfect crystals, such as silicon, germanium and diamond, and installed in a nondispersive scheme. The first crystal collimates and expands the X-rays, producing a pseudo-plane wave that passes through the sample. The phase shift acquired by the X-ray beam upon passing through the sample depends on the thickness of the sample and the number of electrons per unit volume. The phase gradient represents local changes in the direction of the beam, which are resolved by the analyzer. The transmitted X-rays through the analyzer are recorded on an X-ray film. When the analyzer is tuned at an angle inside the Darwin's region, non-refracted X-rays are completely reflected and only refracted X-rays have a chance to pass through the analyzer, leading to the formation of clear dark-field images. On the other hand, when the analyzer is tuned in the vicinity of, but outside, the Darwin's region, both the refracted and non-refracted X-rays pass through the analyzer, leading to the formation of bright-field images. We can thus observe both dark-field and bright-field images by changing the angle of the analyzer. We can also observe absorption-contrast images at angles away from the Bragg condition.

This X-ray optics was tested at a vertical-wiggler beamline, BL-14B. The wavelength of the incident beam was tuned to 0.073 *nm* by the beamline monochromator. The collimator was adjusted at the asymmetric 220 diffraction condition (b = 0.047). The analyzer of 400 μm thickness was adjusted close to the symmetric 220 diffraction condition. At first, we measured the rocking curve of the analyzer, and then recorded the transmitted X-rays through the analyzer on an X-ray film at each offset angle, $\Delta\theta$. The observed area was $9\ mm \times 6\ mm$ in size, and the exposure time was a few seconds. Figure 2 shows the dark-field image observed at $\Delta\theta$ = 1.8" (within the Darwin's region). We could observe both dark-field and bright-field images successfully [1].

Reference

[1] K. Hirano et al., Jpn. J. Appl. Phys. **41**, L595 (2002).

*keiichi.hirano@kek.jp

Fig. 1 Experimental setup

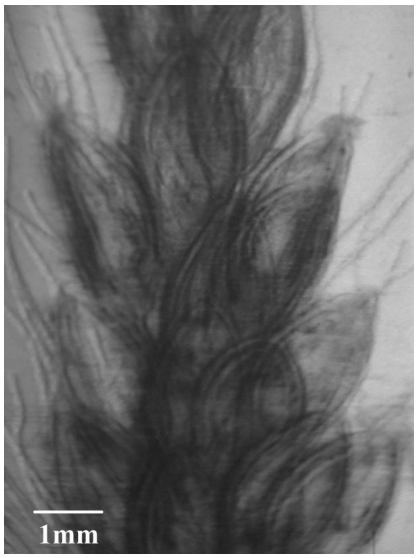

Fig. 2 X-ray refraction-contrast dark-filed image of

18B/2001G146

Crystal structure analysis of malate dehydrogenase

Takeo Tomita[1], Kazuma Yamauchi[1], Nobuyuki Kobashi[2], Makoto Nishiyama[1], Hisakazu Yamane*[1]

[1]Biotechnology Research Center, Unversity of Tokyo, Yayoi, Bunkyo-ku, Tokyo, 113-8657, Japan
[2]RIKEN Harima Institute / Spring-8, Koto 1-1-1, Mikazukicho, Sayo-gun, Hyogo 679-5148, Japan

Malate dehydrogenase (MDH) is the enzyme that catalyzes the last step of the reaction in the tricarboxylic acid cycle and catalyzes the dehydrogenation of malate to produce oxaloacetic acid. MDH has been purified from *Thermus flavus* AT62, and its enzymatic properties have been analyzed[1],[2]. MDH is a dimeric enzyme contains two identical subunits. The gene encoding MDH has been cloned from *Thermus flavus* AT-62 [3].

MDH is an NAD-dependent enzyme. However, the enzyme can catalyze the reaction using NADP as a coenzyme, though the catalytic efficiency is considerably low. We found that K_m value of MDH for oxaloacetic acid markedly increased (200 times), when NADP was used as a coenzyme of MDH [4]. This suggests that NADP binding to MDH induces conformational change around substrate binding site. In order to elucidate the molecular basis of the coenzyme-dependent change in substrate specificity of the enzymatic reation, we tried to determine the structure of MDH/NADP/substrate complexes. Crystals of MDH were grown at 20°C by vapor diffusion in 18~22% PEG 6000, 0.2 M NaCl, 0.1 M Tris-HCl (pH7.5) and 5 mM NADPH. We obtained several crystals of MDH by using a buffer containing NADP and oxaloacetic acid. The obtained crystal was analyzed using BL18B at PF. The space group for the crystal was $P2_12_12_1$. The unit cell parameters for the crystal was a=70.954 Å, b=79.129 Å, c=136.584 Å. The structure analysis revealed that MDH did not contain NADP nor oxaloacetic acid in the molecule. The structure of apo-MDH was nearly identical to that of NAD-binding form of the enzyme.

References
[1] T. Saiki et al., Agric. Biol. Chem. **36** (1972) 2357
[2] S. Iijima et al., Biochim. Biophys. Acta **613** (1980) 1
[3] M. Nishiyama et al., J. Biol. Chem. **261** (1986) 14178
[4] M. Nishiyama et al., J. Biol. Chem. **268** (1993) 4656

*ayamane@mail.ecc.u-tokyo.ac.jp

6A, 18B/2001G151

X-ray crystal analysis of α3β3γε sub-complex of F1-ATPase from a thermophilic bacterium

Yasuo SHIRAKIHARA*[1], Toshiharu SUZUKI[2], Aya SHIRATORI[1], Katsumi MAENAKA[1], Kazuyasu SHINDOH[1], Masasuke Yoshida[2]
[1] National Institute of Genetics, Mishima, Shizuoka 411-8540 Japan
[2] The Chemical Resources Laboratory, Tokyo Institute of Technology, Nagatsuta 4259, Yokohama 226-8503, Japan

Introduction

F1-ATPase, with a subunit composition of α3β3γδε is a catalytic sector of the membrane bound ATP synthase. The ATP synthase plays a central role in energy conversion, generating ATP from ADP and inorganic phosphate using energy derived from a trans-membrane electro-chemical potential. The rotational catalysis mechanism of F1 is accompanied by rotation of the rod-like γ subunit, which is thought to control the conformations of the three catalytic β subunits in a cyclic manner. Using the thermophilic F1-ATPase (TF1), we have been extending the structural study from the α3β3 sub-assembly to the α3β3γδε sub-assembly. In this extension, we aim to detect structural changes caused by different mode of nucleotide binding, which should provide with structural basis for understanding the rotational catalysis mechanism.

The α3β3γδε sub-assembly crystals, when experimented with rotating-anode source, diffracts to 4.5 A resolution at room temperature and 7 A at 100K. With synchrotron beam, we collected a data set to resolution of 4.5 A at 100K. From those figures, the current cooled crystals are thought to be unsatisfactory. While improvement in the cryo-cooling is in progress, we are pursuing to collect the diffraction data at room temperature. In the pervious experiment at BL44 in SP-ring8, we found that the beam (70um in diameter) had to be attenuated by a factor of 300 for avoiding the beam damage and that an IP detector had to be used for the required exposure time much over 1miniute (typically 3 minutes). The results of the experiment was puzzling and disappointing; in one orientation of the plate-shaped crystal, the data extended to only 8 A resolution, and in another orientation (orthogonal to that orientation) the data extended to 4-4.5 A resolution. Those data sets extend at best only marginally compared with the data set obtained in–house.

In this beam time, we made another attempt to collect data at room temperature using the milder beam available at BL18B. We could collect some data sets extending to 3.5 A resolution data, but found problems in collecting the complete data set.

Materials and methods

E. coli Over-expression system for the α3β3γε sub-complex was constructed to allow efficient purification of the sub-complex. The sub-complex was purified with Ni-NTA, DEAE Toyopearl, Phenyl-Toyopearl columns and with additional heat treatment. Crystals of α3β3γε sub-complex were grown at 25℃ by the sitting drop technique. The 5 μl drop contained 9-11 % PEG 6,000, 0.20 M sodium chloride, 0.05 M Tris-sulphate buffer (pH 8.0), 0.5mM ADP, 2mM DTT, 5mM CDTA, 10% (v/v) ethyleneglycol and 10 mg/ml protein, and the 1 ml reservoir contained 16 % PEG 6,000, 0.2 M sodium chloride and 0.05 M Tris-sulphate buffer (pH 8.0), 5mM CDTA, 10% (v/v) ethyleneglycol. Plate crystals (typical dimensions 0.4 mm × 0.3 mm × 0.15 mm) grew in 2 weeks. Crystals are tetragonal, space group I4122, with cell dimensions of a=b=233.3 Å, c=305.3 Å. For data collection at BL18B, the beam was not attenuated. The wavelength was 0.98A, and the ADSC CCD detector was placed at a camera distance of 300mm.

Results and discussions

The suitable exposure time was found to be 90-120sec, depending on crystals, for 1 degree rotation. The diffraction patterns were again more or less dependent on the orientation of the crystal, as observed before (see Introduction). But the dependency was less clear than in the previous experiment. When the x-ray hits the side of the plates, the patterns extended to 3.5-4.5A resolution (3 independent cases). However, when the incident x-ray hits the face of the plates (3 independent cases), the diffraction pattern extended to 4.5-5.0 A resolution. In both cases, the diffraction patterns were recorded covering 30-degree rotation before the radiation damage deteriorated the diffraction limit seriously. Overall, compared to the previous study, the data collection from the crystals at room temperature at BL18B is more practically feasible. The higher resolution of the data (3.5 A vs. 4 A), the less dependence of the resolution of the data on the orientation of the crystals and the more data collected from a single crystal (30 deg. vs. 3 deg.) constitute the reasons. However, the resolution of the data (the best 3.5 A, accompanied by much lower value at unfavorable orientations) is not much better than that obtained from the cooled crystals. We would need a breakthrough for data collection at room temperature.

*yshiraki@lab.nig.ac.jp

6A, 18B/2001G152

X-ray crystallographic analysis of P-450cam operon repressor CamR

Yasuo Shirakihara*[1], Katsumi Maenaka[1,2], Kazuyasu Shindo[2], Hironori Aramaki[3]

[1]National Institute of Genetics, Mishima, Shizuoka 411-8540, Japan
[2]Advanced Research University, Hayama, Kanagawa, Japan
[3]Daiichi College of Pharmaceutical Sciences, Minami-ku, Fukuoka 815-8511, Japan

Introduction

Pseudomonas putida cam repressor (CamR) is a homodimeric protein that binds to the operator DNA (camO) of cytochrome P450cam operon (camDCAB) to inhibit its transcription. The inducer D-camphor binds toward the CamR protein to repress the binding of CamR protein toward the camO, resulting in the activation of the transcription. Based on biochemical studies, there are some interesting binding properties of CamR toward the operator DNA camO and the D-camphor; (1) CamR protein has two domain structure, the N-terminal DNA binding domain which is proposed to have a typical helix-loop-helix motif and to recognize the camO, and the C-terminal regulatory domain which binds the D-camphor to induce the inhibition of CamR binding to camO, (2) two D-camphor molecules can bind to one molecule of homodimeric CamR in a negative cooperative manner, (3) similar amino acid sequence responsible for camphor binding exist in three proteins of the camDCAB; CamR, cytochrome P450cam and purtidaredoxin reductase. In order to clarify the molecular mechanism of the CamR/camO/D-camphor recognition, we are trying to determine the crystal structures of CamR and its complexes with camO and D-camphor.

Result

The recombinant wild-type (wt-camR) and selenomethionyl derivative CamR proteins (SeMet-CamR) have been overproduced in *Escherichia coli* and purified. The wt-CamR was crystallized in two conditions of (1) 12-14% PEG4K,0.1M KCl, 1% Glycerol, 50mM Na-Pipes (pH7.3), with and without 2mM camphor, 15°C, and (2) 1.6M Pi, Na-Pipes(pH6.7), 2mM camphor, 5°C. On the other hand, the SeMet - CamR protein was not crystallized in the above conditions, but was successfully crystallized in two other conditions of (1) 10% MPD, 25mM Na-cacodylate, 20mM $MgCl_2$, pH 6 at 15°C, and (2) 12.5% PEGMME 550, 25mM Na-Pipes, 2.5mM $MgCl_2$, pH 7.3 at 25°C.

The crystals of SeMet-CamR in the condition (1) have large cell dimensions and large mosaicity, it was difficult to solve the structure. On the other hand, the crystals from condition (2) have the P222 space group with the cell dimension, a= 47 Å, b= 87 Å, c= 105 Å, a=b=c=90° (one molecule per asymmetric unit). The crystals of SeMet-CamR were suitable for cryo-experiment by increasing the concentration of PEGMME 550 to 30%. MAD data using the SeMet-CamR crystal were collected at several wavelengths including, 0.9793 Å (peak), 0.9795 Å (edge) and 0.9879 Å (remote) at the beam line BL18B. For all these data sets, 90 image data with an oscillation range of 2 degree were collected utilizing the ADSC CCD detector system.

All diffraction data were autoindexed, integrated and corrected for Lorentz and polarization effects with the program MOSFLM. Scaling and merging of each data in SCALA indicated a p222 space group (Rmerge~12% on data to 3 Å resolution, data completeness= more than 98%). The data collections for the crystals of the wt-CamR with or without the inducer CamR were also done. A full structure determination is in progress.

*yshiraki@lab.nig.ac.jp

6A, 18B/2001G167

Crystal structure analysis of human autocrine motility factor

Nobutada TANAKA*, Hiroshi UEMURA, Yoshio KUSAKABE, Masato KONDO,
Yasuyuki KITAGAWA, and Kazuo T. NAKAMURA
Laboratory of Physical Chemistry, School of Pharmaceutical Sciences, Showa University,
1-5-8 Hatanodai, Shinagawa-ku, Tokyo 142-8555, Japan

Introduction

Autocrine motility factor (AMF) was originally identified by its ability to stimulate directional motility (chemotaxis) and random motility (chemokinetics) of the AMF-producing tumor cells. AMF stimulates cell motility and growth via a receptor-mediated signaling pathway involving morphological changes, receptor phosphorylation, a pertussis toxin-sensitive G-protein activation, inositol phosphate production, protein kinase C activation, and enhanced production of a metabolite of arachidonic acid. Recently, full-length cDNA cloning for both human and mouse AMF receptor (AMFR) genes has been reported and revealed that the AMFR is a novel type of seven transmembrane helix protein.

Primary structure studies (cDNA cloning and amino acid sequencing) have identified human AMF (558 a.a.) as genetically identical to the extracellular cytokines (neuroleukin (NLK) and maturation factor (MF)), and highly homologous to the intracellular enzyme phosphohexose isomerase (PHI). The extracellular cytokines AMF/NLK/MF were originally identified to exist as a monomer in a solution, whereas the intracellular enzyme PHI was known to exist as a dimer in a solution. Recently, crystal structures of bacterial and rabbit PHIs have been reported and showed that both bacterial and rabbit PHI molecules exist as dimer in the crystal. Although the three-dimensional structures and quaternary structures of the intracellular enzyme PHI are now established, little is known of the tertiary structure, quaternary structure and structure-function relationship of the extracellular cytokines AMF/NLK/MF.

Thus the three-dimensional structure of AMF is essential to clarify the structure-function relationship of the extracellular cytokines AMF/NLK/MF and to know how the intracellular enzyme PHI can be secreted and serve as a cytokine.

Experimental

Crystallization

Expression and purification of human AMF were performed as described [1]. Crystals of human AMF were obtained by the hanging-drop vapour diffusion method, as described elsewhere [2]. Briefly, a droplet was prepared by mixing an equal volume of the protein solution containing the 8 mg/ml human AMF, 0.05 M sodium chloride, and 20% (v/v) glycerol in 0.02 M Tris buffer at pH 7.5 and the reservoir solution containing 28% (w/v) polyethylene glycol with a mean molecular weight of 8,000, 0.2 M sodium acetate, and 20% (v/v) glycerol in 0.1 M cacodylate buffer at pH 6.5. The crystals belong to an orthorhombic space group $P2_12_12_1$ with cell dimensions of a = 80.77 Å, b = 107.4 Å, and c = 270.8 Å. Assuming four subunits (two dimers) per asymmetric unit, we obtained a V_M value of 2.32 Å^3/Da, corresponding to a solvent content of 47%.

X-ray data collection

Since the crystallization conditions of human AMF described above contained 20% (v/v) glycerol in both protein and reservoir solutions, X-ray data collection could be performed at cryogenic conditions without the further addition of a cryo-protectant. Crystals in the hanging-drop were directly mounted in nylon loops and flash-frozen in a cold nitrogen gas stream at 100 K just before the data collection. The data collection was performed by a rotation method at 100 K using an ADSC Quantum4R CCD detector with synchrotron radiation (λ = 1.00 Å at beam line 18B of the Photon Factory, Tsukuba, Japan).

Results and Discussion

The crystal structures of the inhibitor-free open form and E4P-bound closed form of human AMF have been determined at 1.9 and 2.4 Å resolution, respectively [3]. These structures have revealed inhibitor-binding sites and conformation changes upon inhibitor binding. In addition, to examine roles of the residues in an inhibitor-binding site, we performed site-directed mutagenesis studies focusing on the cytokine activity of AMF/PHI. The crystal structure analyses and site-directed mutagenesis studies presented here support the hypothesis that there is an inhibition mechanism of AMF cytokine activity by carbohydrate phosphates for which the compound could compete for AMF binding with the carbohydrate moiety of the AMFR, which is a glycosylated seven-transmembrane helix protein.

References

[1] T. Funasaka et al., B.B.R.C. 285, 118 (2001).
[2] H. Uemura et al., Protein Peptide Lett. 8, 317 (2001).
[3] N. Tanaka et al., J. Mol. Biol. 318, 985 (2002).

* ntanaka@pharm.showa-u.ac.jp

15A/2001G176

Cholesterol creates domains in the lipid bilayer matrix of red blood cell membranes

Peter J. QUINN*[1], Claude WOLF[2], Hiroshi TAKAHASHI[3], Satoru UENO[4], Kamen KOUMANOV[5]
[1]Division of Life Sciences, King's College London, London SE2 9NN, UK
[2]Faculte de Medicine Saint Antoine, 27 rue Chaligny, 75571 Paris, France
[3]Dept. Physics, Gunma Univ. Maebashi 371-8510, Japan
[4]Lab. Biomol. Phys., Hiroshima Univ. Higashi-Hiroshima, 739-8528, Japan
[5]Institute of Biophysics, Bulgarian Academy of Sciences, 1113 Sofia, Bulgaria

Introduction

The currently accepted model of the structure of biological membranes is that they are comprised of a lipid bilayer matrix in which the various intrinsic membrane proteins are distributed. Domains of eucaryotic plasma membrane which are insoluble in Triton X-100 at 4°C and enriched in cholesterol and saturated sphingomyelin can be separated from other soluble fractions which contain predominantly unsaturated phospholipids [1,2]. Our initial experiments were designed to determine whether domains could be detected in lipid extracts of biological membranes using diffraction methods.

Materials and methods

Suspensions of red blood cells were incubated in the presence or absence of cyclodextrin. Total polar lipid extracts of the treated and control cells were prepared and dispersed in an equal weight of buffer. The dispersions were examined on Beamline 15A and scattering intensity in the small-angle and wide-angle regions were recorded during a heating scan from 5° to 50°C and a subsequent cooling scan to 10°C at 1°/min.

Results and discussion

The SAXS/WAXS intensities recorded from a lipid dispersion prepared from control cells during an initial heating and subsequent cooling scan is presented in Fig. 1. At 5°C two lamellar reflections are observed characterized by two orders of reflection at the camera length used. The d-spacings correspond to 7.75 and 7.46nm, respectively. The wide-angle region shows a single broad reflection at a spacing corresponding to 0.46nm characteristic of disordered hydrocarbon chains. Upon heating to 50°C the two peaks remain distinct but the repeat spacings decrease by a few Å.

A lipid dispersion prepared from red blood cells treated with cyclodextrin to partially remove cholesterol was subjected to a similar examination and the results are also seen in Fig. 1. This shows a single lamellar phase of 6.85nm present in the dispersion and that the hydrocarbon chains remain in a disordered state throughout the temperature scanning profile.

Clearly cholesterol induces the phase separation of a cholesterol-rich lamellar phase. It is presumed to represent raft domains consisting predominantly of sphingomyelin and cholesterol. Further studies are in progress to characterize the components of the cholesterol-rich phase.

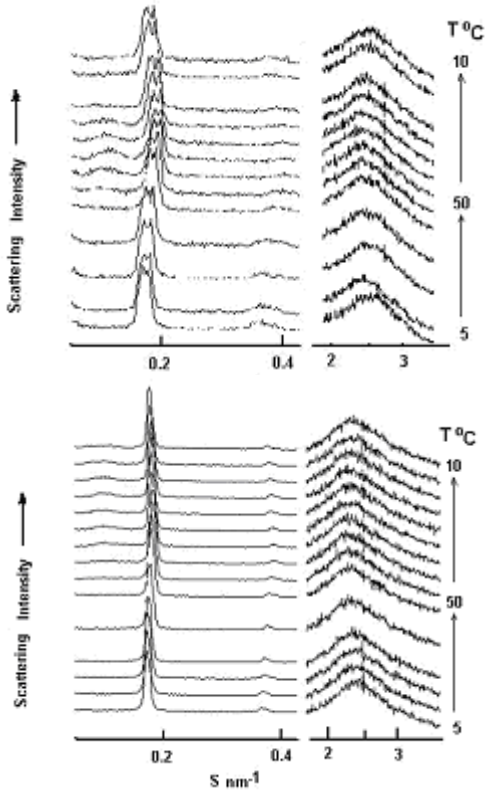

Fig 1. SAXS/WAXS of red blood cell lipids from control (upper) and cyclodextrin treated (lower) cells.

References

[1] D.A. Brown & E. London J. Biol. Chem., **275**, 17221 (2000)
[2] X. Xu & E. London Biochemistry, **39**, 843 (2000).
*p.quinn@kcl.ac.uk

10C/2001G178

Structural study of voltage dependent channel forming peptides in solution

Jun'ichi KATAKAWA*, Tetsuro FUJITA, Chisato ITO, Tadahiro TETSUMI, Yoh SANO
Faculty of Pharmaceutical Sciences, Setsunan University,
45-1, Nagaotoge-cho, Hirakata, Osaka 573-0101, Japan

Introduction

The ion channel study is a very important factor, when it is tried to elucidate the mechanism of an intercellular signal transduction and of an ionic membrane permeability. But it is difficult to discuss the structure-function relations, because the structure analyses of channel-forming proteins do not completely progress yet. So, a low molecular weight model compounds which can form an ion channel may be able to provide useful information. We have the peptaibols [1] (Fig. 1) as one of such the compounds. Hypelcin A-I, antibiotics and hydrophobic peptide, which is one of the peptaibols is taken up in this experiment,

Hypelcin A-I, obtained from *Hypocrea peltata*, is done instrumental analysis, NMR and CD et al., of already [2, 3]. In attempt to obtain further information about structure, we have performed solution small-angle X-ray scattering (SAXS) experiments in various concentrations of hypelcin A-I.

Ac-U-P-U-A-U-U-Q-U-L-U-G-U-U-P-V-U-U-Q-Q-L-OH

Fig. 1 Primary structure of hypelcin A-I

Experimental

Hypelcin A-I was extracted from the stroma of *H. peltata* and purified by chromatography as reported previously [3]. Four sample solutions (30.0, 22.5, 15.0, and 7.5 mg/mL) used for SAXS measurements were prepared by distilled methanol.

SAXS measurements were carried out by using the optics and detector system SAXES (Small-Angle X-ray Scattering Equipment for Solution) were installed at BL-10C in the Photon Factory, KEK. A wavelength of 1.49 Å was used. X-ray scattering intensity was registered at 512 different angles by using the one-dimensional positive proportional counter.

Results and Discussion

Fig. 2 shows the effect of concentration on the scattering intensity in methanol system.

Hypelcin A-I was dissociated to unfold monomer when analyzed by Guinier and Kratky plots. The analysis by Kratky plots and of scattered intensity in relation to weight-averaged molecular weights revealed that hypelcin A-I was completely monomer in methanol solution. The detailed structure and function hypelcin A-I is now analysing from the scattering curves shown in Fig. 2. In fact, hypelcin A-I takes the helical structure and behaviors as rod like molecules in solution.

These results were in good agreement with the results of CD data and the channel conductance method suggesting the bundle of ideal a-helical structure.

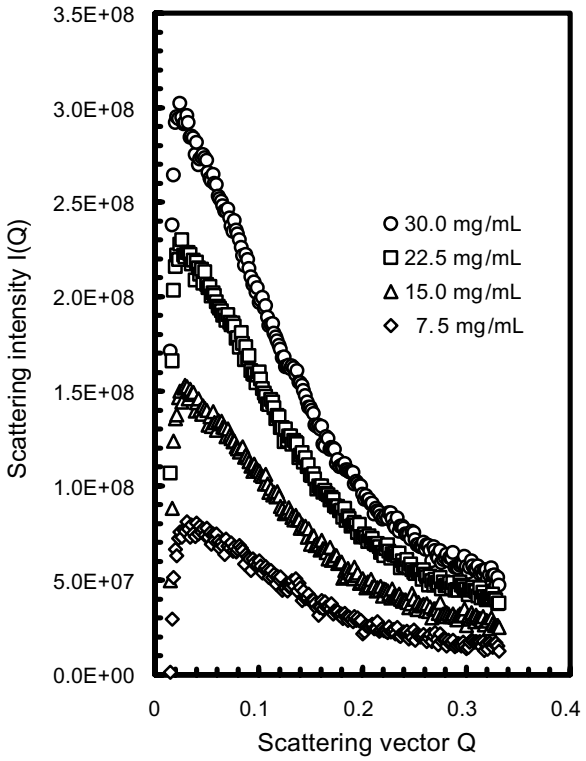

Fig. 2 The effect of concentration on the scattering intensity in methanol system.

References

[1] H.Brückner and M. Przybylski, *J. Chromatogr.*, **296**, 263 (1984).
[2] K. Miyajima et al., Biochemistry, **28**, 9392(1989).
[3] T. Fujita et al., J. Chem. Soc., Perkin Trans. **1**, 381(1993) .
*katakawa@pharm.setsunan.ac.jp

4A/2001G179

Investigation of differentiation of mouse ES cells

Ari Ide-Ektessabi[*1], Shunsuke Shikine[2], Shigeyoshi Fujisawa[2], Takuo Kawakami[2], Koyo Shirasawa[2]
[1]International Innovation Center, Kyoto Univ., Yoshida Honmachi, Sakyo-ku, Kyoto 606-8501, Japan
[2]Graduate School of Engineering Kyoto Univ., Yoshida Honmachi, Sakyo-ku, Kyoto 606-8501, Japan

Introduction

Embryonic stem (ES) cells are expected to bring the breakthrough in the therapy for progressive neurodegenerative disorders such as Parkinson's disease, Alzheimer disease and Huntington disease. ES cells are generally called pluripotent stem cells and are unique in that they have the capacity for unlimited self-renewal along with the ability to produce multiple different types of terminally differentiated descendants. The differentiation of ES cells can be controlled in vitro by choosing the configuration of culture conditions. Although the procedure to induce neuronal differentiation is partly revealed, the details of mechanism are unknown. Therefore it remains quite difficult to culture neurons efficiently for therapeutic application.

In this study, x-ray fluorescence (XRF) analysis was applied to investigate the mechanism of differentiation by dissecting the change of distributions and concentration of intracellular trace elements in mouse ES cells [1,2]. It is considered that trace metal elements and metalloproteins are deeply related to the orientation of differentiation as active centers as well as the neural cell death in neurodegenerative disorders.

Experimental Set ups and Sample Preparation

The SR-XRF analyses in this investigation were performed at Photon Factory in beam line 4A. The incident x-ray energy was 14.3 keV and the beam size was approximately 7 x 5 μm^2. The analyses were carried out in air.

The mouse ES cells (129/Sv) were purchased from Cell & Molecular Technologies, Inc. and the passage number (the age of cell line) was 15 in the beginning of the cell culture. Samples for the elemental analysis were prepared by fixing colonies that had been cultured on Mylar films with 20% formalin solution. Three and two samples are made at the passage number 16 and 17.

Results and Discussions

The elemental distribution were obtained in the three or four areas that contained colonies in each sample. The typical image of Zn of the sample at the passage number 17 is shown in Fig. 1. The scale on right side of the image shows the count of the x-ray intensity. The typical spaectra obtained in the colonies are shown in fig. 2. It is suggested that chlorine and zinc had increased according to the differentiation. The concentration of Zn had increased from 0.07 to 0.09 and those of Cl had decreased from 0.67 to 0.14 in the average of relative amounts to P during the change of the passage number. The difference among concentration of these elements is considered to be deeply related to the biological functions such as proliferation, gene transcription and cell excitability in the process of the differentiation.

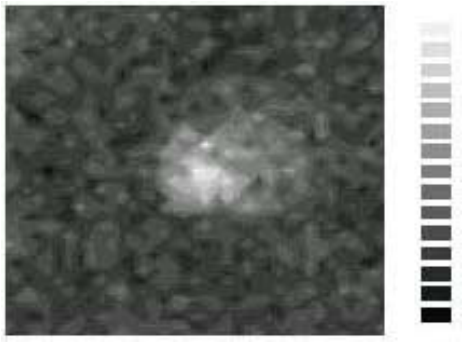

Fig. 1. The typical image of Zn obtained in the mouse ES cell colony at the passage number 17. Measurement area was 144 x 144 μm^2 and the measurement time was 6sec/point.

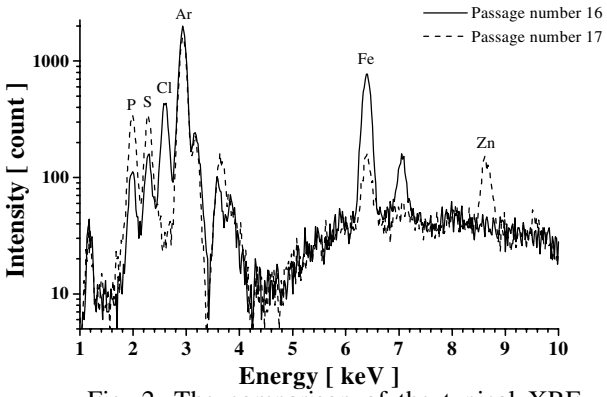

Fig. 2. The comparison of the typical XRF spectra obtained in the mouse ES cell colonies at the passage number 16 (solid line) and 17 (dotted line). The measurement time was 200sec.

References

[1] Rpbertson JA, Nature Reviews Genetics 2, 74 (2001).
[2] Fraichard A et al., J. Cell Sci. 108, 3181 (1995).

* h51167@sakura.kudpc.kyoto-u.ac.jp

6A/2001G339

X-ray crystallographic study of V_1-ATPase

Noriyuki ISHII*
Biological Information Research Center, National Institute of Advanced Industrial Science and Technology, Tsukuba Central-6, 1-1-1 Higashi, Tsukuba, Ibaraki 305-8566, Japan

Introduction

V-type ATPase belongs to a class of ATP-driven proton pumps responsible for acidification of intracellular compartments in the cells. Although it had been believed that all H^+-translocating ATPases in prokaryotic cells are F_0F_1-ATPases, some kinds of eubacteria as well as most archea have been found to hold V_0V_1-ATPases whose role is ATP synthesis coupled with proton flux across membranes. V_0V_1-ATPases consist of two functional sectors (as does the F_0F_1-ATPase) designated as a peripheral V_1 moiety and an integral membrane V_0 moiety.

The proton translocating ATPase found in the plasma membrane of an aerobic thermophilic eubacterium, *Thermus thermophilus*, belongs to the class of V_0V_1-ATPases. The V_1 moiety from *T. thermophilus* HB8 consists of four subunits with a stoichiometry of $A_3B_3\gamma_1\delta_1$. The molecular masses of the individual subunits are approximately 66 (*A*), 55 (*B*), 30 (γ) and 11 kDa (δ), respectively[1].

A structural comparison at high resolution between V- and F-type ATPases would elucidate the common features involved in biological energy by which ATP synthesis/hydrolysis reaction is coupled to proton translocation across a membrane.

Experimental

Prior to the crystallization, the protein solution was incubated in the presence of 5 mM Mg-ADP at 328 K for 10 minutes. Crystallization conditions were screened by use of the sparse-matrix approach. The hanging drop vapor diffusion method was employed throughout the crystallization study. The crystallization procedure was as follows; 2 µl of a solution containing 16.2 mg/ml *Thermus* V_1-ATPase in 20 mM Tris-HCl pH 7.2, and the same volume of a reservoir solution were equilibrated against 500 µl of reservoir at 298 K for 2-3 weeks. The reservoir solution contained 100 mM sodium acetate, 2 M sodium formate, and 5 mM Mg-ADP, adjusting pH to 5.5.

The obtained crystals were mounted in cryo-loops followed by rapid dipping through a buffer containing the same components as the reservoir solution plus 30 % glycerol as a cryo-protectant. Intensity data were collected at 105 K using synchrotron radiation at the BL-6A. Oscillation photographs were taken by the ADSC Quantum 4R CCD detector. The data were processed using DPS/MOSFLM and programs from the CCP4 suite.

Results

Crystals of *Thermus* V_1-ATPase with approximate dimensions of 36 × 36 × 143 µm were frequently obtained. Larger sized crystals were rare and was probably due to the tendency of V_1-ATPase to unfold at the interfaces, forming a film of unstructured polypeptides that inhibited further equilibration.

Preliminary intensity data were collected in which the diffraction extended beyond 3.4 Å resolution. The data indicated that the crystals belong to the trigonal space group *P*3. The unit cell dimensions were determined as a = b = 89.0 Å, c = 179.2 Å, and γ = 120°. Assuming that the unit cell contains one molecule of V_1-ATPase with a molecular mass of 404 kDa, the V_m value is calculated as 3.0 $Å^3$/Da, and corresponds to a solvent content of 59.6 %.

The initial processing of data has been restricted to the diffraction range of 20 - 6.5 Å, due to the anisotropic nature of the diffraction data obtained. There still remain several possibilities to assign the space group within the hexagonal system, such as *P*6, $P6_3$, $P6_322$, as well as to the trigonal system *P*3. The peripheral portion (hexagon) composed of the large subunits, *A* and *B*, may strongly dominate the diffraction data, especially if the small γ and δ subunits are located with some disorder, as has been described for the atomic model of mitochondrial F_1[2]. Recognizing that the *A* and *B* subunits are highly homologous but not identical, and that there are only single copies of the γ and δ subunits in the V_1 moiety, we have to be aware that the (pseudo-) symmetrical axis just suggested may be limited only to the low and middle resolution range. I thus conclude that the space group of *P*3 is the one that most likely describes the current resolution range (20 - 6.5 Å)[3]. The unit cell dimensions seem reasonable from the view of the molecular size of V_1-ATPase, and from a comparison with the previously reported dimensions for the crystals of F_1-ATPases[2, 4].

According to the report[1], the crystals that I obtained and described above are likely to contain V_1-ATPase molecules in the Mg-ADP-inhibited form. Thus, the structure analysis of this crystal form may help to understand the manner in which Mg-ADP associates with and inactivates V_1-ATPase during ATP hydrolysis. The crystals obtained under these condition can be used for structure determination at higher resolution. The further optimization of crystallization conditions is in progress, along with intensity data collection and structure determination.

Acknowledgement

I thank Drs. T. Sato, N. Tanaka and K. Harata for discussion.

References

[1] K. Yokoyama et al., J. Biol. Chem. 273, 20504 (1998).
[2] J.P. Abrahams et al., Nature 370, 621 (1994).
[3] N. Ishii et al., J. Struct. Biol. 134, 88 (2001).
[4] Y. Shirakihara et al., Structure 5, 825 (1997).

* ishii@ni.aist.go.jp

6A/2001G346

Crystal structure analysis of an autoregulator-receptor protein in *Streptomyces* species

Ryo NATSUME[1], Shin MURAOKA[2, 3], Yutaka FURUSAWA[1,3], Toshiya SENDA*[3]
[1]The University of Tokyo, 1-1-1 Yayoi, Bunkyo-ku, Tokyo 113-8657, Japan
[2]Nagaoka University of Technology, Nagaoka, Niigata 940-2188, Japan
[3] BIRC, AIST, 2-41-6 Aomi, Koto-ku, Tokyo 135-0064, Japan

Introduction

The gram-positive bacteria genus *Streptomyces* is characterized by the ability of its metabolites and by complex morphological differentiation. A-factor is a chemical signaling molecule, or a microbial hormone, that is essentially required for aerial mycelium formation, streptomycin production, streptomycin resistance, and yellow pigment production in *Streptomyces griseus*. A-factor binding protein shows high specificity to A-factor and has a repressor-type function. Upon binding with A-factor, A-factor binding protein appears to dissociate from the promoter region of its target genes resulting in an activation leading to transcription of the genes. This A-factor/ArpA like system is considered to be a common regulatory system controlling secondary metabolism and morphogenesis of the *Streptomyces*. CprB is a homologue protein of ArpA found in a closely related microbe, *Streptomyces coelicolor* A3(2). In order to gain an insight into the mechanism of the regulatory system, we have tried to solve the crystal structure of CprB with the MAD method. However, the MAD electron density (3.2Å resolution) cannot be interpreted fully, as the quality of the electron density map was poor. To obtain a better electron density map, we have tried to collect high-resolution diffraction data of the CprB crystal. Here we report a high-resolution crystal structure analysis of CprB.

Results

The CprB was overexpressed using *E. coli* and purified to near-homogeneity by three steps of chromatographic procedure. Crystallization of CprB was carried out using the typical hanging drop vapour diffusion method. The crystals grew to the dimensions of 0.3mm x 0.3mm x 0.05mm at the maximum. The high-resolution data was collected at 100K using an ADSC Quantum CCD detector at BL6A of PF. The CprB crystal belonged to the space group $P2_12_12_1$ with the cell dimensions of a = 37.8Å, b = 69.6Å, c = 148.9Å. All the data were processed using the program DPS/MOSFLM and scaled with the program SCALA in the CCP4 program suite. The statistics of the data collection is shown in the Table 1.

Table 1 Statistics of data collection

Resolution (Å)	29.7 - 1.8
Rmerge (%)	4.1
Completeness (%)	85.4
Multiplicity	3.9
I/sigma(I)	11.7

Since the cell parameters of the present crystal were significantly different from those of the crystal using in the MAD phasing, the crystal structure was determined by the molecular replacement method (MR). A masked electron density corresponding to one CprB molecule, which is derived from the MAD analysis, was used as an initial model, as no reasonable molecular models of CprB were available. The MR analysis gave a clear result, and the obtained electron density map was of enough quality, resulting in the complete model building of CprB. The crystallographic refinement is in progress. The present R-factor is 25.7% (FreeR=27.1%) at 2.0Å resolution.

The crystal structure of CprB shows that CprB is a dimeric protein as predicted by biochemical analysis. The subunit has a DNA-binding domain (residues 1 to 52), and a cofactor-binding domain (residues 53 to 212). The CprB molecule is an alpha-helical protein with no apparent beta-strands in its structure.

10C/2001G366

Characterization of transient intermediates of a calmodulin-peptide complex 2

Yoshinobu IZUMI*[1], Yuji JINBO[1], Tomohiro MATSUFUJI[1], Hidenori YOSHINO[2], Yuzuru HIRAGI[3], Hiroshi KIHARA[4]
[1]Graduate School of Science and Engineering, Yamagata University, Yonezawa 992-8510, Japan
[2]Department of Chemistry, Sapporo Medical University, Sapporo 060-8556, Japan
[3]Institute for Chemical Research, Kyoto University, Uji 611-0011, Japan
[4]Department of Physics, Kansai Medical University, Hirakata 573-1136, Japan

Introduction

We have previously reported that the EDTA-induced dissociation processes of Ca^{2+} ions from a complex of Ca^{2+}-saturated calmodulin ($4Ca^{2+}$/CaM) with Ca^{2+}/CaM-dependent protein kinase IV peptide (CaMKIVp) is characterized by biphasic kinetics[1], suggesting that the first event is the loss of two Ca^{2+} ions from the N-terminal lobe, followed the loss of two Ca^{2+} ions from the C-terminal lobe [2].

In the present work we have measured the dissociation kinetics of a complex of $2Ca^{2+}$ /CaM with CaMKIVp. The result obtained is compared with that calculated from an equimolar mixture of $4Ca^{2+}$/CaM/CaMKIVp and $0Ca^{2+}$/CaM/CaMKIVp. We confirm again that the rate of the slowest step is determined by the contribution of a kinetic relaxation mechanism involving the intermediate species, which have been previously suggested [2].

Materials and Methods

A 19-residue peptide having the sequence (CaMKIVp: RRKLKAAVKAVVASSRLGS) and recombinant CaM were used. Stopped-flow experiments were performed using an instrument for SAXS with a stopped-flow apparatus (Unisoku Co.Ltd) at BL10C of PF.

Results and Discussion

The result in Fig. 1 indicates that the molecular weight of the CaM-peptide complex does not change during the dissociation process, suggesting that the peptide binds to CaM even in the absence of Ca^{2+}, which is supported by a recent report [3]. Furthermore, the dissociation pathway is characterized by monophasic kinetics as shown in Fig. 2, in which the result corresponds to the loss of two Ca^{2+} ions from the C-terminal lobe. The experimental value of Rg at t=0 is 19.7A, while the calculated value under the condition in which $4Ca^{2+}$/CaM/CaMKIVp (Rg=17.6A) and $0Ca^{2+}$/CaM/CaMKIVp (Rg=20.3A) equally exist, is 19.1A. The significant difference indicates the existence of the intermediate species and supports the contribution of a kinetic relaxation mechanism involving them. From the Rg value, it is suggested that the conformation of $2Ca^{2+}$/CaM/CaMKIVp is a dumbbell-like structure similar to $4Ca^{2+}$/CaM/CaMKIV.

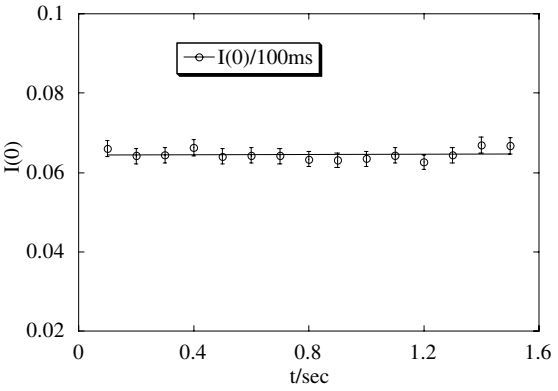

Fig. 1 Time course of the forward scattering amplitude I(0) for the dissociation of $2Ca^{2+}$/CaM/CaMKIVp complex.

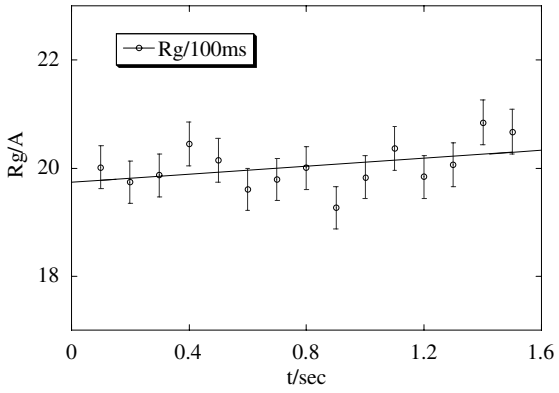

Fig. 2 Time course of the radius of gyration Rg for the dissociation of $2Ca^{2+}$/CaM/CaMKIVp complex.

References

[1] Y.Izumi et al., PF Activity Rep. 2000 B18, p.235.
[2] S.E.Brown et al., J.Biol.Chem. 276 3389(1998).
[3] Y.Izumi et al., FEBS Lett. 495, 126(2001).
* yizumi@yz.yamagata-u.ac.jp

BL15A1/2001G368

A small angle X-ray scattering study of ClpA and ClpP from *Escherichia coli*

Yoshihiko Igarashi*[1], Kazumoto Kimura[1], Shigeru Matsuzaki[1], Hiroshi Kihara[2], Singh Satyendra[3], Michael Maurizi[3]
[1]Dokkyo Univ., Mibu Tochigi 321-0293, Japan
[2]Kansai Medical Univ., Uyamahigashi Hirakata Ohsaka 573-1136, Japan
[3]National Cancer Institute/NIH, Bethesda, MD 20892-4255, USA

Introduction

ATP-dependent proteases play a major role to maintain proper protein homeostasis, contributing to protein quality control and modulating the intracellular concentration of important global regulatory proteins. *Escherichia coli* has several soluble ATP-dependent proteases, Lon, ClpAP and ClpXP. ClpAP degrades *E. coli* denaturated L-glutamate dehydrogenase (GDH) to maintain the cell growth at starved condition [1]. ClpAP is a complex of two heterologous proteins, ClpA, which catalyzes the ATPase activity, and ClpP, which contains the proteolytic active site. Molecular properties of ClpA and ClpP have been studied by hydrostatic methods [2] and electron microscopy [3]. ClpA made a hexameric structure that had Mr 505k in the presence of ATP and ATP analogs. ClpP had subunits arranged in double rings of seven-subunit rings [2,3] that had molecular weights of 300k. Tetradecamer of ClpP was determined only by samall angel X-ray scattering [4]. We try to show that the structure of *E. coli* monomer or dimmer and hexamer of ClpA and heptamer and teteradecamer of ClpP in various solutions using small angel X-ray scattering (SAXS) method.

Materials and Methods

ClpA and ClpP were purified separately as described briefly. ClpA was overexpressed in mostly soluble form in *E. coli* CSH 100 under very strong promoters p_{tac} on multicopy plasmids pSK-39. ClpA was purified as a mixture of monomeric and dimeric forms in 50 mM Tris/pH7.5 /1 mM EDTA/10% (v/v) glycerol /0.2 M KCl. ClpP has been cloned under the control of T7 promoter in a pET3a plasmid and expressed in *E. coli* strain SG1147 clpA::kan. ClpP can be overproduced in a soluble form [5]. Purified ClpP was associated tetradecamer in 50 mM Tris-HCl, pH 7.5, containing 0.2 M KCl .

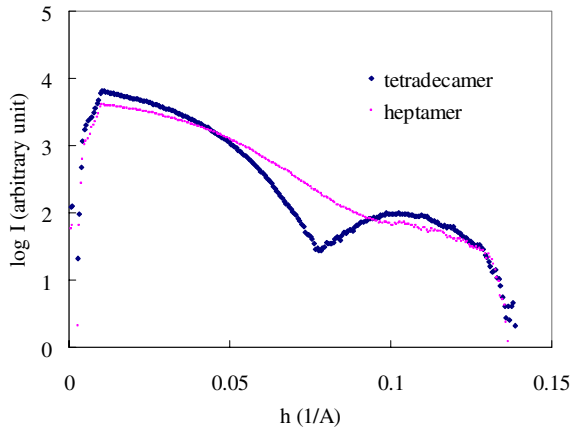

Figure Scattering patterns of ClpP tetradecamer and heptamer

Small-angle X-ray scattering (SAXS) experiments were performed at BL-15A1. The sample solution was irradiated with monochromatic X-rays (1.504 A) and scattered X-ray intensities were recorded on a two-dimensional CCD-based X-ray detector with a camera length of 2342 mm and channel width of 0.307 mm. The raw SAXS data were corrected for intrinsic image distortion, non-uniformity of response and contrast reduction. After image distortion correction, the 2-dimensional data were translated to 1-dimensional data (512channels) using circular averaging.

Results and Discussion

ClpA

Rg of ClpA showed 63 Å in the presence of 2 mM ATPγS. There were no subpeaks in the scattering pattern of ClpA. It seems that ClpA structure would not have one rigid structure. One may not get a clear data similar to electron microscopy results of Kessel, M. *et al*.,[3]

ClpP

When ClpP was present with >0.1 M KCl at pH 7.5 at room temperature, ClpP was tetradecamer. After ClpP was put into 20 mM sodium phosphate, pH 7.2, with 0.1 M sodium sulfate at 5 C, ClpP was dissociated into heptamer. Rg values of tetradecamer and heptamer were 45 and 36 Å respectively. The cube of ratio of Rg was 2:1, directly proportional to the molecular weight.

The results of these ClpPs scattering patterns are shown in the Figure. The tetradecamer of ClpP has some ordered structures at inside of ClpP but ClpA did not show any ordered structures.

References

[1] M. Maurizi *et al*., Arch Biochem Biophys **397**,206 (2002)
[2] M. Maurizi *et. al*., Biochemistry **37**, 7778 (1998)
[3] M. Kessel *et al*., J. Mol. Biol. **250**, 587(1995)
[4] J. Flanagan Biocheistry **34**, 10910 (1995)
[5] M. Maurizi *et al*., *Methods Enzymo*l. **244**, 314 (1994)

*bioiga@dokkyomed.ac.jp

15A/2001G369

An X-ray solution scattering study on the conformation of skeletal muscle myosin subfragment-1 in the presence of Mn^{2+} and ATP

Tomohiro OKUMURA[1], Toshiaki ARATA[2], Yasunobu SUGIMOTO[1], Yasunori TAKEZAWA[1], Maya KIYOTOSHI[1], and Katsuzo WAKABAYASHI*[1]

[1]Division of Biophysical Engineering, Graduate School of Engineering Science

[2]Department of Biology, Graduate School of Science, Osaka University, Toyonaka, Osaka 560-8531, Japan

Introduction

The conformations of the skeletal muscle myosin subfragment-1 (S1, the myosin head) of the intermediate states in the ATPase cycle have extensively been investigated by solution X-ray scattering. It has been suggested biochemically that the predominant intermediates of the Mn^{2+}-dependent myosin S1 ATPase are applicable to the S1*· MgADP complex at low temperatures (< 10 °C) [1]. In order to define the magnitude and extent of the changes, the conformations of S1 in the presence of Mn^{2+} and ATP were examined by X-ray solution scattering.

Experimental

Papain-digested myosin subfragment-1 was prepared from the rabbit skeletal myosin molecules. Purified S1s through a column chromatography were centrifuged and used for X-ray experiments. Mn^{2+} and ATP were added to the S1 solution to make the final concentration of Mn^{2+} and ATP were 6 mM and 3 mM, respectively. X-ray experiments were done at 4 °C and 20 °C at the BL15A1. All scattering data were collected with a 1D-PSD.

Results and Discussion

The Guinier plots of the scattering intensity data (I(S)) from the S1 solution in the presence of Mn^{2+} and ATP gave all straight lines. The I(0)/c versus c (protein concentration) plots were also linear. Figure 1 shows the concentration dependence of the radius of gyration (Rg) values of the samples, compared with those from several reference samples. The true Rg value of S1 in the presence of Mn^{2+} and ATP was ~50 Å at 4 ℃, ~2 Å larger than that of the nucleotide-free S1 while it was ~48 Å at 20 ℃, comparable to that of the nucleotide-free S1. The Rg value of S1 in the MgATP solution was ~46 Å, corresponding to S1**· MgADP·Pi. The scattering intensity profile of S1 ($I(S)\cdot S^2$ versus S plot) (in the range of $S > 0.01$ Å^{-1}) in the presence of Mn^{2+} and ATP at 4 °C moved toward smaller S than those of the other samples but at 20 °C was close to that of the nucleotide-free S1 (Fig. 2). Interestingly, both of the Rg value and the whole scattering curve of S1 in the MnATP solution resembled closely to those of the pPDM-crosslinked S1 trapping MgADP (S1· MgADP-pPDM) [2].

It has been suggested that at low temperature S1*· MgADP comprises a greater proportion of the steady-state complex in the Mn^{2+}-dependent ATPase of S1 [1]. The present results provide two possibilities: (1) the conformation of the S1*· MgADP in the ATPase cycle of S1 is different from that assumed by S1 by sole addition of MgADP, (2) the conformation of S1 in Mn^{2+} and ATP solution at low temperature globally resembles to that of S1· MgADP-pPDM where the light chain-binding domain of S1 moves in the opposite direction to that in the S1**· MgADP·Pi. The results at room temperature may be applicable to an equilibrium mixture of S1*· MgADP and S1**· MgADP · Pi.

References

[1] C. R. Bagshaw, FEBS Letters, **58**, 197 (1975).

[2] Y. Sugimoto et al., PF Activity Rep., #18, 233 (2000).

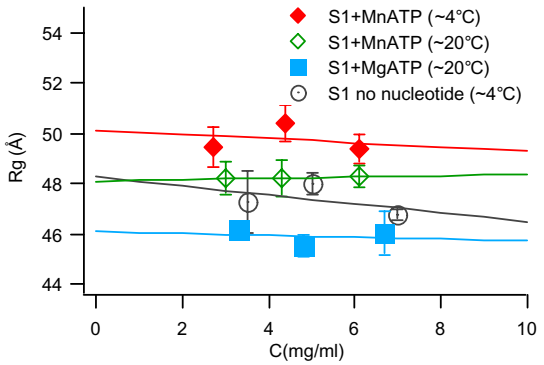

Fig.1 The concentration dependence of Rg values of S1 in the presence of Mn^{2+} and ATP solution, compared with those of other samples.

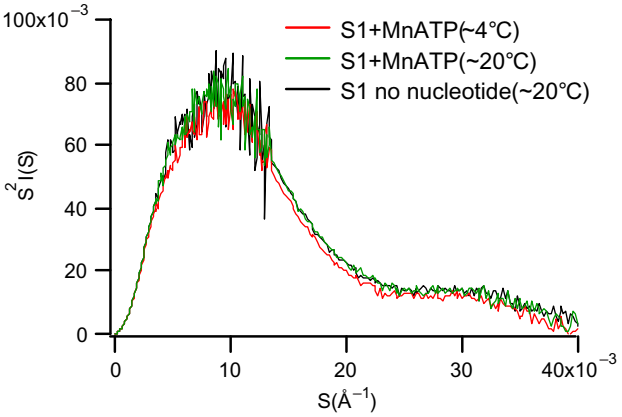

Fig. 2 The Kratky plots of scattering data of S1 in various solutions.

*waka@bpe.es.osaka-u.ac.jp

15A/2001G370

Alteration of the helical twist associated with the shortening of the thin actin filaments upon activation of skeletal muscles

Yasunori TAKEZAWA[1], Yasunobu SUGIMOTO[1], Takakazu KOBAYASHI[2], Kanji OSHIMA[1] and Katsuzo WAKABAYASHI*[1]
[1]Division of Biophysical Engineering, Graduate School of Engineering Science, Osaka University, Toyonaka, Osaka 560-8531, Japan
[2]Department of Physiology, School of Medicine, Teikyo University, Itabashi-ku, Tokyo 173-0003, Japan

Introduction

Twisting changes of the actin helical structure associated with its filament extensibility upon activation of frog skeletal muscles stretched to non-overlap length of thin and thick filaments were investigated by measuring the axial spacing of the actin-based first layer-line component in the X-ray diffraction pattern. In the first layer-line complex, the thin and thick filament-based components could be resolved in the radial region close to the meridian, by a Gaussian deconvolution method [1]. We inspected the axial spacing change of the first actin layer line together with those of the actin 5.9-nm and 5.1-nm layer lines upon activation.

Experimantal

Living semitendinosus muscles of the bullfrog were used for this study. We measured 2D X-ray diffraction patterns from muscles stretched to non-overlap length of thin and thick filaments in resting and activated states. X-ray experiments were performed at BL15A. The 2D diffraction patterns were recorded on image plates. The specimen-to-detector distance was ~2m.

Results and Discussion

There appeared two layer-line components in the very inner radial region (0.020 R 0.039 nm^{-1}); one component located at ~1/38.0 nm^{-1}, almost the same axial level as the first troponin-related meridional reflection and the other sit at ~1/42.9 nm^{-1} which was the myosin-based first layer line. The axial spacing of the 38.0-nm component decreased by ~0.10% upon activation of an overstretched muscle, similar to the average spacing change of the troponin-related meridional reflections. Thus, this component originates from the troponin molecules, associated with the first troponin-related meridional reflection. In the next inner region (0.039 R 0.063 nm^{-1}), there existed a diffuse and weak component centered at ~1/36.6 nm^{-1}, which sit at the axial level higher than at 1/38.0 nm^{-1} and seemed to be the actin-based component. Upon activation it decreased in spacing by ~1.38% below its resting value. The 5.9-nm and 5.1-nm layer lines, corresponding to the pitches of the left- and right-handed genetic helices of the monomer in the actin filament, decreased respectively in the axial spacing by ~0.01% and ~0.15% below their resting values upon activation. The observation that the spacing change of the 5.1-nm reflection was larger than that of the 5.9-nm reflection was consistent with our previous reports [1][2]. Figure 1 summarizes the spacing changes of the inner and next inner regions of the first actin layer line together with those of the 5.9-nm and 5.1-nm actin layer lines. The spacing decrease of the first actin layer line estimated from those of the 5.9-nm and 5.1-nm layer lines was ~1.18% (a white bar graph), close to the observed spacing change of the 36.6-nm component, as above. The spacing decrease of the actin-based 2.7-nm meridional reflection estimated from those of the 5.9-nm and 5.1-nm reflections was ~0.09%. This was also very close to the observed change in our previous experiments where the overstretched muscles were activated [2][3]. These results confirmed that the shortening of the thin actin filament caused by the activation was closely associated with a twisting change of the right-handed helices of the actin filament.

References

[1] Takezawa et al., J Mus. Res. and Cell Motil., **22**, 205 (2001).
[2] Wakabayashi et al., Biophys. J., **67**, 2422–2435 (1994).
[3] Takezawa et al., Adv. Exp. Med. & Biol., **453**, 309–317 (1998).

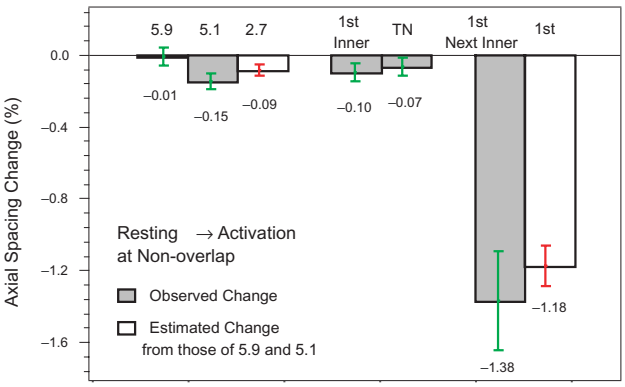

Fig.1 Spacing changes of the first actin layer-line components and the troponin meridional reflections (TN), together with those of the 5.9-nm and 5.1-nm layer lines.

* waka@bpe.es.osaka-u.ac.jp

15A/2001G372

Study of uracil DNA glycosylase complexes with ligands by synchrotron X-ray scattering

Alexander TIMCHENKO[1], Elena KUBAREVA[2], Hiroshi KIHARA*[3]
[1] Institute of Protein Research, Pushchino, Russia, 142292;
[2] Institute of Physico-Chemical Biology of Moscow State University, Russia, 117333;
[3] Dept. of Physics,Kansai Medical University Uyamahigashi, Hirakata Osaka 573-1136, Japan

Introduction

Uracil DNA glycosylase (UDG) is a key enzyme in the DNA repairing system. The last X-ray analysis data [1] of UDG from different origins elucidated the high specificity of this enzyme to uracil base produced by cytosine deamination in DNA. The large changes of DNA conformation are observed at UDG action. We decided to test large-scale conformational changes of UDG in solution upon ligand binding by synchrotron X-ray scattering.

Experimental

UDG was isolated from the M15 strain (REP4) of *E.coli* carried the pR632 plasmid. The buffer conditions are: 20mM Tris-HCl (pH7.6), 60mM NaCl, 1mM EDTA. Protein concentration was 5.5 mg/ml (0.21mM). Free protein and its complexes with $(pT)_3$ inhibitor (c=0.87mM), with 18-mer non-hydrolyzable oligonucleotide (c=0.36mM), with 14-mer oligonucleotide (c=0.36mM) and their duplex (c=0.36mM) have been studied Synchrotron X-ray measurements were done on a small-angle camera BL-15A (Photon Factory, Tsukuba)

Results

Guinier plot were not linear reflecting the protein association preferably in dimer form. Evaluated radii of gyration (Rg) were (2.27+/–0.1)nm for free protein, (2.10+/–0.1)nm for UDG+$(pT)_3$, (2.34+/–0.1)nm for UDG+18-mer, (2.35+/–0.1)nm for UDG+14-mer, (2.68+/–0.1)nm for UDG+duplex. For globular protein of 26 kD molecular mass the expected Rg doesn't exceed 2nm. Fig.1 shows the distance distribution function P(R) for all studied samples. One can see the essential compactization of protein upon $(pT)_3$ binding and partial distruction of protein associates what correlates with our previous data on His-tag UDG. Such destruction is also observed for oligonucleotides in contrary to duplex action. Evaluation of molecular masses shows that in all cases the complexes are formed and their dimensions increase with the molecular mass increase what is evident from the shift of maximum on P(R). In contrast to His-tag UDG UDG with native sequence is globular. Further analysis of data will permit to elucidate the conformational changes in UDG upon ligand binding.

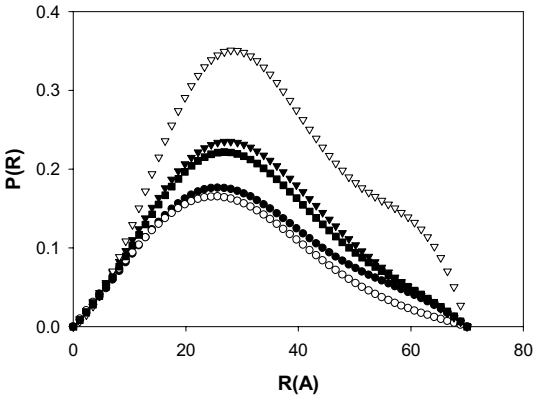

Fig.1 P(R) for UDG (●), UDG+$(pT)_3$ (○), UDG+18-mer (▼), UDG+14-mer (■), UDG+duplex (▽).

References

G.Slupphaug et al., Nature **384**, 87, 1996

*kihara@makino.kmu.ac.jp

10C/2001G375

Fibrillation of human calcitonin as studied by solution x-ray scattering

Tadashi TOMIZAWA [1], Yasutaka SEKI [2], Yuzuru HIRAGI [3], Kunitsugu SODA [*4]
[1] GSC, RIKEN, Yokohama, Kanagawa 230-0045; [2] Div. Biol. Sci., Grad. Sch. Sci., Nagoya Univ., Nagoya, Aichi 464-8602; [3] Inst. Chem. Res., Kyoto Univ., Kyoto, Kyoto 611-0011; [4] Dept. Bioeng., Nagaoka Univ. Technol., Nagaoka, Niigata 940-2188, Japan

Introduction

Human calcitonin (hCT) is a peptide hormone with 32 amino acid residues and is known to form fibrous aggregates as β -amyloid. In this study, fibrillation of hCT at neutral pH and with high protein concentration has been analyzed by solution x-ray scattering (SXS) method, where time dependence of the average degree of association and the global shape of aggregates were measured. Combined with results of other experiments and molecular modeling, SXS study would contribute greatly to elucidate the fibrillation mechanism of proteins.

Method

SXS experiment has been done using the PF beam line BL10C. Time dependence of the SXS profile of hCT at a concentration of 10 mg/ml has been measured at acidic pH 2.0 (10mM HCl) and neutral pH 6.0 (10mM HEPES). To minimize the damages of sample protein molecules by x-ray irradiation, SXS measurement has been made flowing continuously the sample solution through a sample cell. The actual x-ray irradiation time of each hCT molecule is 0.5 s. SXS data were accumulated for 5 minutes. The SXS profile of the protein in each sample was obtained by subtracting the SXS profile of solvent from that of solution.

Result

The upper figure shows the Kratky plot for an acidic hCT solution of pH2.0. The mean square radius R_{sq} of hCT was found to be 1.3 nm from Guinier analysis. Comparison of the forward scattering intensity between hCT and myoglobin confirmed the monomeric form of hCT. Under this solution condition, no change in the SXS profile was observed within 90 minutes after sample preparation. As seen from the upper figure, hCT in acidic solution has a random-coil structure, which is consistent with the result of CD-spectrum measurement.

Kratky plots of the SXS profile at neutral pH 6.0 are presented in the lower figure. The profiles in the figure are normalized with the forward scattering intensity of monomeric hCT. The plots of a, b, c and d are respective profiles at 5, 80, 95 and 165 minutes after the sample preparation. No change in the SXS profile was observed within 80 minutes after the dissolution of hCT into solvent. As the forward scattering intensity and the value of R_{sq} in this range of time coincide with those observed under the acidic condition, hCT just after dissolving into neutral solvent is found to have monomeric, random coil

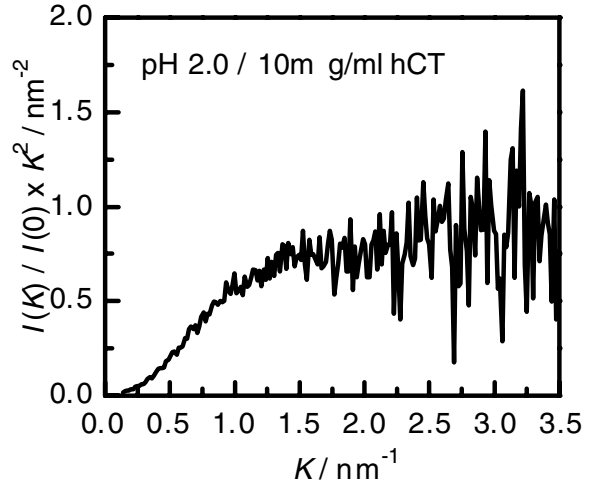

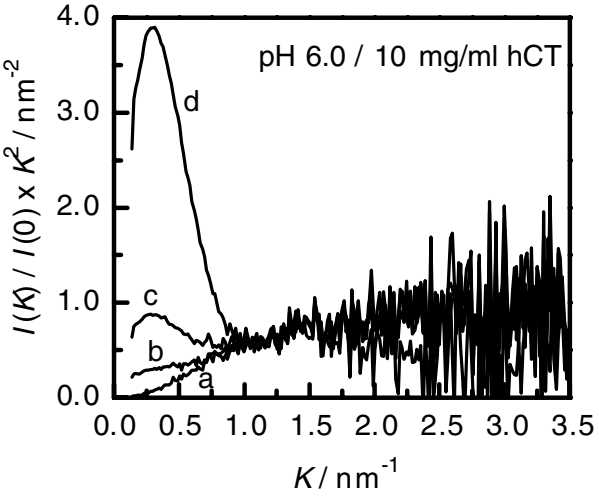

conformation. The scattering intensity suddenly increases at 80 minutes after dissolution to yield finally the profile as shown in the plot d. It was found after the SXS measurement that the sample solution geled and resonance Raman scattering measurements showed that hCT molecules have conformations rich in β -strand. Combined with results of CD measurement, these SXS data shows that the fibrillation of hCT proceeds with the nucleation of some hCT oligomer followed by growth of the fibril. Detailed analysis of the SXS profiles is now in progress.

References

[1] Y. Seki, T.Tomizawa, N.N. Khechinashvili and K. Soda, Biophys. Chem. **95**, 235-252 (2002).

* soda@vos.nagaokaut.ac.jp

15A/2001G376

Analysis of unfolding and refolding of HIV protease

Kayoko TAKEUCHI[1], Hiroyuki KOGO[1], Hideshi INOUE[1], Yon-Tae KIM[2], Xin-Li LIN[2], Yoshiyuki AMEMIYA[3], Hiroshi KIHARA[4], Masaki KOJIMA*[1], Kenji TAKAHASHI[1]
[1] School of Life Sci., Tokyo Univ. of Pharm. & Life Sci., Hachioji, Tokyo 192-0392, Japan
[2]Oklahoma Med. Res. Fdn., Oklahoma City, Oklahoma 73104, USA
[3] Graduate School of Frontier Sci., Unv. of Tokyo, Bunkyo-ku, Tokyo 113-8656, Japan
[4]Dept. of Physics, Kansai Med. Univ., Hirakata, Osaka 573-1136, Japan

Introduction

HIV-1 protease is an acid proteinase, and is essential for the maturation of the infectious virions. It consists of two identical subunits with 99 residues, which are bound non-covalently (Fig. 1). Like other acid proteinases such as pepsin and aspergillopepsin II, the enzyme is unfolded at higher pH. In order to elucidate the unfolding profiles of HIV-1 protease, small angle X-ray scattering (SAXS) experiments were performed.

Experimental

All the measurements were performed at BL-15A with a CCD-based X-ray detector [1] at 20°C.

HIV-1 protease was expressed in *E.coli* and purified by the method reported previously [2]. Sample solutions were prepared by diluting 2-fold the enzyme solution (7.3 mg/ml in 10 mM Na acetate, pH 3.5) with 10mM Na MES (pH 5.5) or 10 mM Na CAPS (pH 10.0). All sample solutions contained 1 mM dithiothreitol.

The data were corrected for distortion of images, non-uniformity of sensitivity, and contrast reduction of an X-ray image intensifier [3] before analyses.

Results and Discussion

Fig. 2 shows the SAXS pattern of HIV-1 protease in the native state (pH 3.5). Radius of gyration (R_g) was estimated to be 19.1 A from the Guinier approximation, and the Kratky plot indicated that the molecule was globular in the native state. On the other hand, the SAXS pattern in the unfolded state suggested that there were some aggregates in the sample solution. This may be because the two subunits dissociated at alkaline pH could easily form aggregates. We are now investigating the relationship between unfolding of HIV-1 protease and its aggregation.

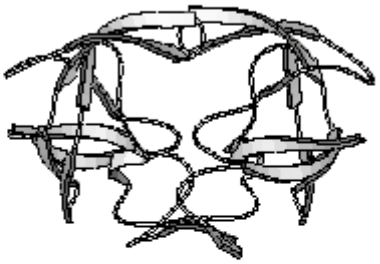

Fig. 1. Schematic representation of the structure of HIV-1 protease [4].

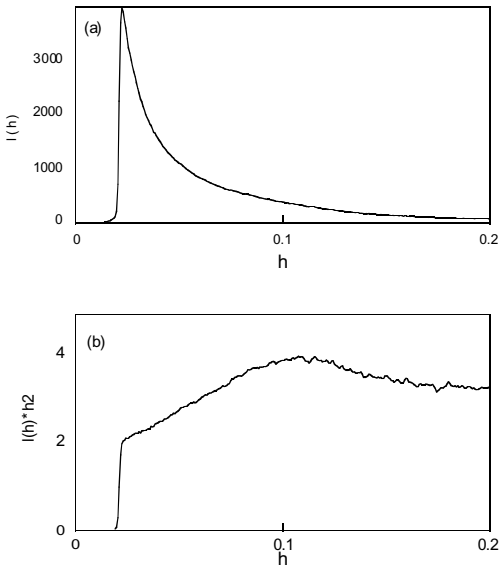

Fig. 2. SAXS profile (a) and Kratky plot (b) of HIV-1 protease at pH 3.5

References

[1] Y. Amemiya et al., Rev. Sci. Instrum. **66**, 2290 (1995).
[2] E. Ido et al., J. Biol. Chem. **266**, 24359 (1991).
[3] K. Ito et al., PF Activity Report **18**, 275 (2001).
[4] A. Wlodawer et al., Science **245**, 616 (1989).

*mkojima@ls.toyaku.ac.jp

11A/2001G378

Improvement of spatial resolution in soft X-ray projection microscope

Atsushi ITO*[1], Kunio SHINOHARA[2], Toshio HONDA[3], Misako SAITO[3], Rumiko KURIYAMA[3], Hideyuki YOSHIMURA[4], Hiroshi MAEDA[4], Ayumi HORI[4], Hisamitsu ENDOH[5], Takashi KOMATSUBARA[5], Masato ACHIHARA[5], and Yasuhito KINJO[6]
[1]School of Engineering, Tokai Univ., Hiratsuka-shi, Kanagawa 259-1292, Japan
[2]Graduate School of Medicine, Univ. of Tokyo, Bunkyo-ku, Tokyo 113-0033, Japan
[3]Faculty of Engineering, Chiba Univ., Chiba-shi, Chiba 263-8522, Japan
[4]School of Science and Technology, Meiji Univ., Kawasaki-shi, Kanagawa 214-8571, Japan
[5]Faculty of Engineering and Design, Kyoto Inst. Technol., Kyoto 606-8585, Japan
[6]Tokyo Metropolitan Industrial Technol. Res. Inst., Setagaya-ku, Tokyo 158-0081, Japan

Introduction

We have been developing a projection microscopy system using synchrotron radiation, where an intense X-ray point source is produced by a Fresnel zoneplate[1]. The resolution was improved and estimated to be around 0.2 μm. However, the test pattern for this estimation was found to be inappropriate for precise determination, because a periodical pattern having many lines could produce pseudo-line images probably due to the overlapped Fresnel fringes. In the present study, we re-examined the spatial resolution using a new test pattern with much fewer lines of a defined width. Furthermore the obtained images were subjected to image processing including iteration procedure for reconstruction of a real image from an image accompanying Fresnel fringes[2]. These trials confirmed that the spatial resolution is better than 0.25 μm at the present status.

Materials and Methods

Monochromatic soft X-rays of 1.5 nm wavelength were obtained at the beamline 11A. A typical optical layout of the projection microscopy was illustrated in Fig. 1. A pinhole behind the zone plate was installed to remove the higher order diffracted light, and a pre-pinhole before the zone plate, which was placed at the focal point of the focusing toroidal mirror installed at the downstream of the monochromator, was used for improving spatial coherence of incident light to the zone plate.

Spatial resolution was evaluated using a test pattern with grooves of defined widths (Silson Ltd, England).

Reconstruction procedure of an image with Fresnel fringes is basically identical to that used for the in-line holography. The procedure was previously developed for the reconstruction of images of specimens having a totally dark surrounding restriction area[2]. We used the method with some modification.

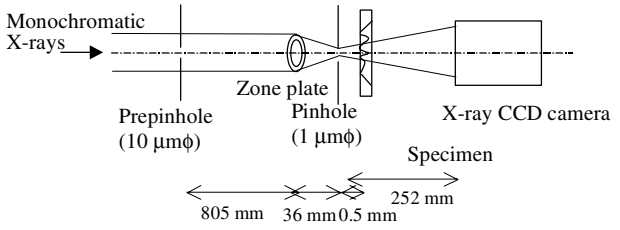

Fig. 1. Layout of projection X-ray microscope.

Results and Discussion

Figure 2 shows an X-ray image of the test pattern taken under the condition of 1 μm pinhole with 10 μm pre-pinhole. The test pattern has four sets of vertical and horizontal lines with 0.5, 0.25, 0.1 and 0.05 μm. The image was blurred with Fresnel fringes, showing no apparent pattern structure except the 0.5 μm section.

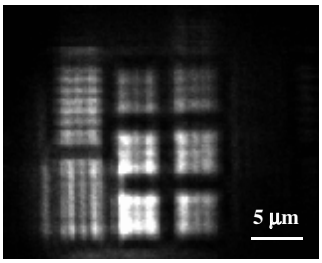

Fig. 2.
X-ray image of a test pattern with lines and spaces of defined widths taken at 1.5 nm.

However, after image processing the 0.25 m section was clearly resolved, indicating that the iteration method is effective. These results demonstrated that the resolution of the present projection microscope achieved at least 0.25 μm with the aid of image processing.

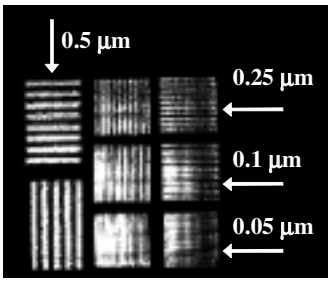

Fig. 3.
Reconstructed image of a test pattern.

References

[1] K. Shinohara et al., In "X-RAY MICROSCOPY", (edited by W. Meyer-Ilse et al.), pp. 346-349, New York: American Institute of Physics, (2000).
[2] K. Shinohara et al., J. Synch. Radiat., 3, 35-40 (1996).

* aeito@keyaki.cc.u-tokai.ac.jp

15A/ANBF

Changes in the diffraction patterns of hair samples resulting from increased airport and postal security checks post September 11, 2001.

Veronica James*
Research School of Chemistry, Australian National University, Canberra ACT 0200, Australia

Abstract

A subset of the samples examined at the Advanced Photon Source, Chicago, in late 2001 yielded unusual changes in the fibre diffraction patterns. This report confirms that these changes were not related to the BioCAT Facility at the APS but were directly related to either the changes in the radiation of hand-luggage resulting from the increased security measures at the airport in Los Angeles or to the irradiation of mail within the United States.

Introduction

In a double blind study of 160 hair samples at the BioCAT Facility, Advanced Photon Source, Argonne National Laboratory, Chicago,(APS) the fibre diffraction patterns obtained for all samples, that had been transported from Australia or had been sent by post within the USA, were different from the pattern for normal hair. Figure 1.

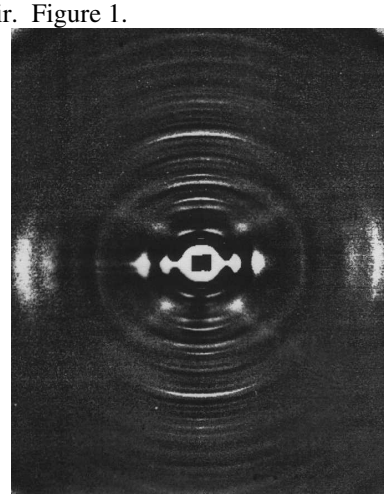

Figure 1. Fibre diffraction pattern for human controls.

This change was not the same as that already reported for hair of persons known to have breast cancer or insulin dependent diabetes, [1][2][3]. After the double blind was revealed for the Australian samples, the majority of these samples were revealed to be normal and not abnormal. In addition it was revealed that hair from a number of these samples had been examined on at least one previous occasion and had yielded the expected normal patterns. Either the problem had occurred in transit or at the BioCAT facility. The latter was unlikely as the samples that were couriered from within the USA to APS appeared to be unaffected. It had been observed that notices at the hand luggage radiation check points in Los Angeles stated that this radiation would affect all film in contrast to the regular signs in Sydney and other airports that state that only film with ASA values greater than 1000 will be affected. This study was designed to establish the origin of these changes.

Materials and Method

Further hairs were taken from all samples that had exhibited the change at APS. In this case, however, multiple samples were used. Ten to twenty hairs were used dependent on the number of hairs available. These samples were examined on beam-line BL15A using the method reported for earlier experiments using multiple samples[4]. Some new samples known to be normal were taken from Australia and were also examined..

Results

All new normal samples gave the same patterns as Figure 1. However those that had been carried through the Los Angeles airport or sent through the USmail showed similar changes to those observed at BioCAT.. Figure 2.

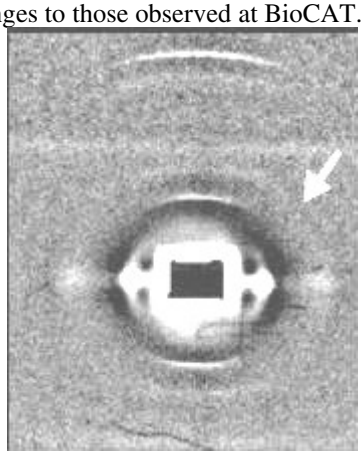

Figure 2. Normal hair after irradiation at Los Angeles airport, the arrow indicates the wide fuzzy arcs that appeared on all the diffraction patterns

Conclusion

Whilst this eliminated BioCAT as the source of the problem and confirms that some damage to the samples has occurred, a further study is needed to verify that the increased radiation measures are the direct cause. From other studies, it is known that both gamma rays and microwaves will affect hair.

Acknowledgments

The assistance of Professors K.Wakabayashi and Y.Sugimoto in setting up the beam-line, the support of the Photon Factory, the ASRP and the ANPF staff were much appreciated.

References

1P..Meyer et al J..Nat.Can.Inst.**93**(11),873 (2001)
2.V.James et al, Nature,**308,**(6722),33 (1999)
3. V..James et al, Biophys Biochim Res.Com. 233, 76 (1997)
4.K.Wilk et al.,Biochim. Biophys. Acta 1245,392(1995)

*vjs@bigpond.com